Australasian Physical & Engineering Sciences in Medicine (2019) 42:3–25
https://doi.org/10.1007/s13246-019-00730-z

REVIEW PAPER

Multiparametric MRI and radiomics in prostate cancer: a review

Yu Sun[1,2] · Hayley M. Reynolds[2] · Bimal Parameswaran[3] · Darren Wraith[4] · Mary E. Finnegan[5,6] · Scott Williams[2] · Annette Haworth[1]

Received: 19 June 2018 / Accepted: 22 January 2019 / Published online: 14 February 2019

Abstract

Multiparametric MRI (mpMRI) is an imaging modality that combines anatomical MR imaging with one or more functional MRI sequences. It has become a versatile tool for detecting and characterising prostate cancer (PCa). The traditional role of mpMRI was confined to PCa staging, but due to the advanced imaging techniques, its role has expanded to various stages in clinical practises including tumour detection, disease monitor during active surveillance and sequential imaging for patient follow-up. Meanwhile, with the growing speed of data generation and the increasing volume of imaging data, it is highly demanded to apply computerised methods to process mpMRI data and extract useful information. Hence quantitative analysis for imaging data using radiomics has become an emerging paradigm. The application of radiomics approaches in prostate cancer has not only enabled automatic localisation of the disease but also provided a non-invasive solution to assess tumour biology (e.g. aggressiveness and the presence of hypoxia). This article reviews mpMRI and its expanding role in PCa detection, staging and patient management. Following that, an overview of prostate radiomics will be provided, with a special focus on its current applications as well as its future directions.

Keywords Prostate cancer · Multiparametric MRI · Radiomics · Machine learning · Tumour · Heterogeneity

Introduction

Multiparametric MRI (mpMRI) is an imaging modality that combines anatomical MR imaging with one or more functional MRI sequences and has become an important tool for detecting and characterising prostate cancer (PCa) [1]. The traditional role of mpMRI was confined to PCa staging, but due to the advanced imaging techniques, its role has expanded to tumour detection, disease monitor during active surveillance and patient follow-up. Meanwhile, with the growing speed of data generation and the increasing volume of imaging data per patient, development of computerised methods to process mpMRI data and extract useful information is highly demanded. Take tumour delineation for example, manual delineation of tumour location is associated with subjectivity and inter-observer variation. In a study by Steenbergen et al. [2], tumour delineations on mpMRI (T2w imaging, DWI and DCE-MRI) from six observers using data from 20 patients were compared and results showed the median inter-observer standard deviation (SD) was 0.23 cm and 69 satellites lesions were missed by all observers. Such inter-observer variability can affect the reproducibility of clinical procedures and hence compromise the consistency of treatment delivery. The second factor which has contributed to the development of computer-aided systems is the availability of a large number of features available in mpMRI. The traditional way to detect potential lesions is by manually looking at multiple images including parametric maps, but this is only practical with small sets of images. Recent studies on medical image processing have identified the great value of a variety of image features in detecting and characterising PCa [3, 4]. The number of feature maps can easily reach into the tens if not hundreds of features, which means qualitative manual assessment is not practical and quantitative assessment using computerised methods becomes necessary. Hence quantitative analysis for

✉ Yu Sun
yu.sun@sydney.edu.au

1 University of Sydney, Sydney, Australia
2 Peter MacCallum Cancer Centre, Melbourne, Australia
3 Imaging Associates, Melbourne, Australia
4 Queensland University of Technology, Brisbane, Australia
5 Imperial College Healthcare NHS Trust, London, UK
6 Imperial College London, London, UK

imaging data using radiomics has become an emerging paradigm. The application of radiomics approaches in prostate cancer has not only enabled automatic localisation of the disease but also provided a non-invasive solution to assess tumour biology (e.g. aggressiveness) down to the genetic level.

This article reviews mpMRI and its expanding role in PCa detection, staging and patient management. Following that, an overview of prostate radiomics (using conventional machine learning techniques) will be provided, with a special focus on its current applications as well as its promising future directions.

Multiparametric MRI

The attempt to use MRI to define tumour location for PCa dates back to the 1980s when trials were carried out using anatomical T1-weighted and T2-weighted images, but they did not succeed due to a lack of sensitivity and specificity [5]. During the last three decades, the accuracy of tumour detection has increased by combining anatomical imaging and functional MRI (e.g. diffusion weighted MRI and dynamic contrast enhanced MRI) [6]. The use of mpMRI has emerged as a better way to evaluate PCa, providing substantial improvements in tumour detection. To-date, mpMRI is the only imaging modality that has both the spatial resolution and soft-tissue contrast necessary to characterise PCa [7]. In 2013, the European Society of Urogenital Radiology (ESUR) developed guidelines termed the Prostate Imaging-Reporting and Data System (PI-RADS) to standardise the use of mpMRI in imaging PCa [8]. An updated version (PI-RADS v2) was released in 2015 by a joint committee including the American College of Radiology (ACR), ESUR and the AdMeTech Foundation [9]. For mpMRI sequences, PI-RADS v1 recommended T2-weighted imaging, diffusion-weighted imaging, dynamic contrast enhanced MRI and MRS [8], while PI-RADS v2 removed MRS as a recommended sequence [9]. PI-RADS (both v1 and v2) provides a system using a Likert-like five-grade scoring system to evaluate the relative likelihood of the existence of a clinically significant PCa [10–14]. The PI-RADS score ranges from one, which is described as "clinically significant disease is highly unlikely to be present", to five which means "clinically significant cancer is highly likely to be present" [8, 9, 15]. This section introduces the relevant mpMRI sequences in PCa detection and how each sequence is used in PI-RADS for PCa detection.

T2-weighted imaging

T2-weighted (T2w) imaging provides high-resolution anatomical information of the prostate. The zonal anatomy and capsules can also be well depicted on T2w images, as the peripheral zone (PZ) typically has intermediate to high signal intensity (SI) [7]. T2w images are suitable for identifying the tumour lesion as well as assessing seminal vesicles, neurovascular bundles and prostate margins for extraprostatic extension. It is difficult to distinguish between the transition zone (TZ) and the central zone (CZ) on T2w images; hence they are grouped together and called the central gland (CG). PCa in the PZ typically has lower SI than the surrounding tissue due to its higher cell density (Fig. 1). However, low SI is not specific for PCa as various conditions such as prostatitis, haemorrhage, atrophy and post-treatment changes can result in similar patterns in T2w images [8].

Tumours in the transition zone (TZ) often appear as a homogeneous signal mass with indistinct margins (Fig. 1) and a lenticular (or "water-drop") shape [8] as opposed to the more heterogeneous appearance of glandular and stromal prostatic hyperplasia which occurs more commonly in the TZ. Detection accuracy for TZ tumours decreases as the baseline SI of normal prostate tissue is lower [16] and images patterns are commonly confounded by benign prostatic hyperplasia (BPH) [17], a non-cancerous enlargement or growth of the prostate gland. Previous studies have also

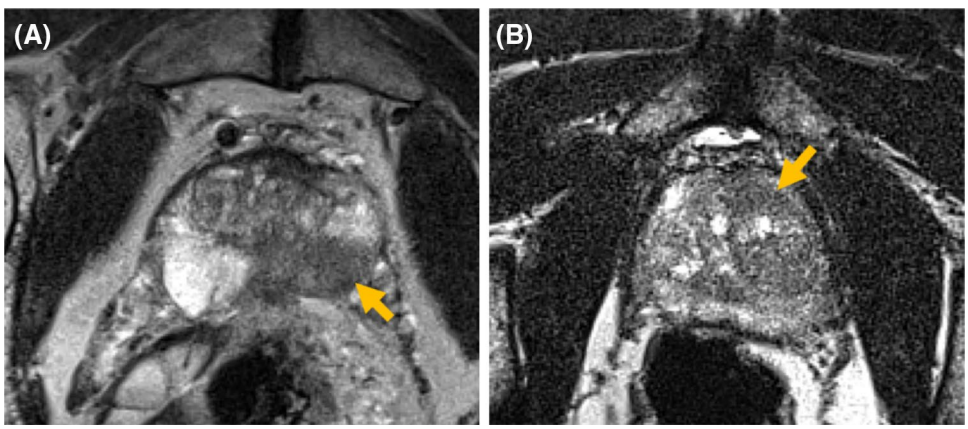

Fig. 1 T2w images showing **a** a peripheral zone lesion and **b** a transition zone lesion. Arrows point to the lesion locations

investigated using calculated T2 values to assess the concentration of citrate (a PCa biomarker) [18–20] but relevant reports are scarce.

In summary, despite various useful features, T2w imaging is limited by the low specificity and a lack of reliability under certain circumstances [21, 22]. Hence T2w imaging is used in conjunction with other functional imaging techniques in mpMRI. For the TZ, T2w imaging is the primary determining sequence (dominant technique) in PI-RADS v2.

Diffusion-weighted imaging

Diffusion is caused by the random motion of water molecules, also known as the Brownian motion. In a cellular environment, water diffusion is hindered by cellular components such as cell membranes and organelles within the cytoplasm, which can cause restricted diffusion. The degree of diffusion restriction is related to the microstructure of the tissue. A higher degree of diffusion restriction is usually found in tumours compared with healthy tissues [23]. This formed the basis for using diffusion-weighted imaging (DWI), a non-invasive imaging modality, for detecting cancer since the 1990s.

DWI data can be assessed in two different forms: using the raw diffusion-weighted images or the computed apparent diffusion coefficient (ADC) images [24]. When acquired with more than one b value (a parameter to define diffusion sensitisation), ADC maps can be computed using the following equation:

$$ADC = -\frac{\ln\left(\frac{S_1}{S_0}\right)}{b_1 - b_0}, \quad (1)$$

where S_0 and S_1 are the SI obtained with b values b_0 and b_1, respectively. The ADC provides a quantitative measure for water diffusion, which is related to the underlying microstructure of the tissue (e.g. cellularity) [25]. It has been shown that incorporation of ADC maps with T2w images (area under the curve, or AUC = 0.887 and 0.732 for two readers) outperformed using T2w images alone (AUC = 0.859 and 0.662, respectively) in detecting intermediate-risk and high-risk PCa [26], since PCa has lower ADC values than healthy prostate tissue [8]. In addition, ADC has shown correlation with cellularity [25] and tumour aggressiveness in PCa [25, 27–31]. Figure 2 shows an example of a T2w image and the corresponding ADC map where tumour shows decreased ADC values.

In addition to ADC maps, raw diffusion-weighted images acquired with high b values (> 800 s/mm^2) are also discriminative in depicting PCa as tumours have higher signal intensity, both in the PZ and the CG [8]. Recently, the use of very high b values has been investigated. Wang et al. compared the performance of ADC obtained using b values up to 2000s/mm^2, and found that a b-value at 1500s/mm^2 offered the highest efficiency in PCa detection [32]. This was consistent with another study by Rosenkrantz et al. that a b-value between 1500 to and 2500s/mm^2 were optimal [33]. However, this requires further validation in clinical procedure. Figure 3 shows an ADC map and a high b-value diffusion-weighted image of the same tumour. It has been shown that incorporating diffusion-weighted images with T2w images significantly improves the performance of PCa detection (AUC = 0.93) compared with using T2w images alone (AUC = 0.87) [34, 35].

Dynamic contrast enhanced MRI

Dynamic contrast enhanced MRI (DCE-MRI) is an MRI technique used to characterise vascular properties of tissue. It involves injecting a contrast agent into a patient so that the dynamic uptake of the contrast agent within the tissue

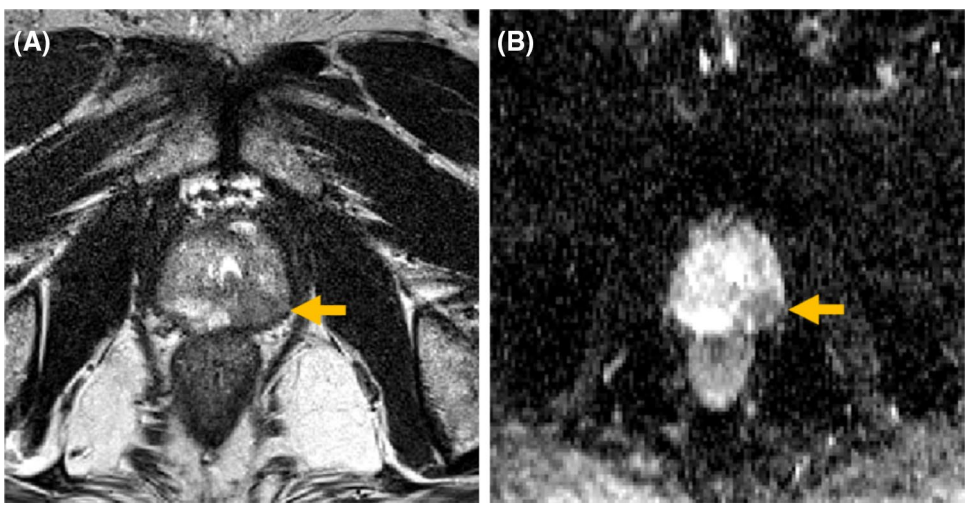

Fig. 2 An example of a tumour on **a** a T2w image and **b** an ADC map (computed using b values of 50, 400, 800, 1200 s/mm^2) showing a decreased ADC value. Arrows indicate the tumour location

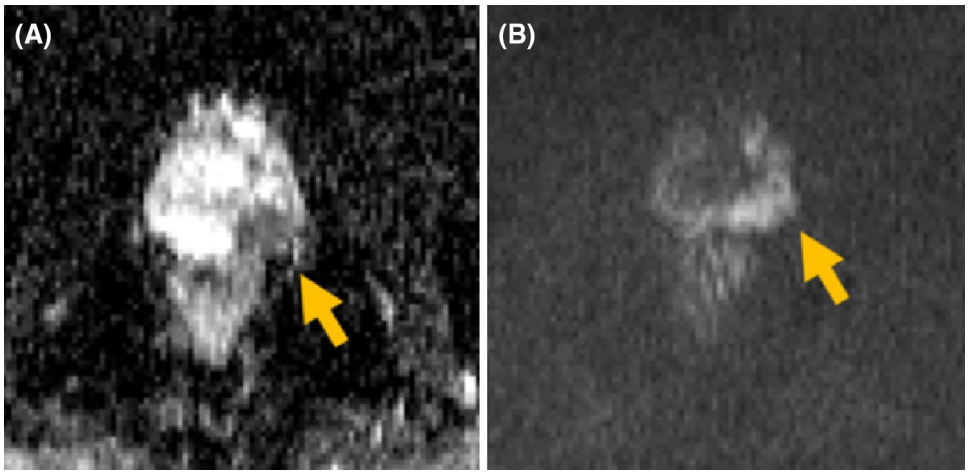

Fig. 3 An example of **a** an ADC map (computed using b values of 50, 400, 800, 1200s/mm^2) and **b** a DWI image (b = 1200s/mm^2) with the lesion pointed by the arrow. The tumour shows a decreased value on the ADC map and an increased intensity on the DWI image

of interest can be observed. Similar to other cancers, PCa generally shows faster uptake (enhancement) and washout compared with healthy tissue [36, 37], due to the angiogenesis associated with tumours which stimulates and facilitates the growth of blood vessels [38]. Compared to normal vessels, the permeability of tumour blood vessels is typically higher due to the weak integrity of the vessel wall [39–41]. The increased permeability of tumour blood vessels mediates metastasis and previous studies found that prognosis worsens as the number of abnormal vessels in PCa increased [42, 43].

DCE-MRI involves the acquisition of a series of 3D T1-weighted images following an intravenous injection of a bolus of contrast agent. The contrast agent is usually a low-molecular weight gadolinium-based chelate, which shortens local relaxation times and hence increases the SI on T1-weighted images [44]. The contrast agent extravasates from the blood vessels to the extravascular extracellular space (EES, also called 'leakage space') then back to the vessel before being cleared by the kidneys [45]. This causes the T1 signal to first increase and then decrease, which forms a dynamic curve for a particular voxel. The PI-RADS guidelines recommend a temporal resolution of 5 s per acquisition, with a maximum of 15 s [8]. A comparison between static T1 images before and after the injection of contrast agent is not sufficient to discriminate PCa and normal tissues: an analysis of the dynamic uptake curve is necessary [46, 47].

There are three approaches to analyse DCE-MRI data: qualitative, semi-quantitative and quantitative (Fig. 4). Qualitative analysis (also known as curve type analysis) relies on visual examination of DCE-MRI data. PCa typically shows a rapid signal enhancement after injection of the contrast agent followed by rapid washout. Normal tissues, on the other hand, show slower enhancement and continuously declining signal at washout. However, this approach is not widely adopted due to the reported subjectivity and poor performance [48]. To improve objectivity and reproducibility, semi-quantitative methods have been developed which calculate parameters from the dynamic uptake curve; these include the rates of wash-in, rate of wash-out, and the time to peak enhancement. Though these simple features can be discriminative for detecting PCa [49–51], there is a lack of standardisation regarding the features to be computed in semi-quantitative methods. In addition, semi-quantitative features can be affected by the temporal resolution of the DCE-MRI acquisition. These limitations can be resolved by applying quantitative methods, which use predefined pharmacokinetic models to compute features. Commonly used pharmacokinetic models for DCE-MRI data analysis include the Tofts model [52], the Brix model [53] and the Larsson model [54]. Despite the concern that DCE-MRI may add to the cost and inherent risks of mpMRI, due to use of contrast agent, multiple studies have demonstrated the value of DCE-MRI in complementing T2w imaging and DWI, as well as assessing cancer aggressiveness and helping identify recurrence after treatment [55].

MR spectroscopy

MR spectroscopy (MRS) utilises the different resonant frequencies, or chemical shift, of hydrogen nuclei in different chemical environments to probe metabolite concentrations in tissue. Multi-voxel MRS can be used to look for metabolite changes associated with tumour cells in within the prostate. Previous studies have shown that PCa is associated with an increased concentration of choline and a decreased concentration of citrate and spermine [56–58], which can be detected using MRS. Despite its diagnostic value, MRS is limited by long scanning times [8], low spatial resolution [58] and high propensity for artefact. Therefore PI-RADS v2 has downgraded MRS from a recommended sequence

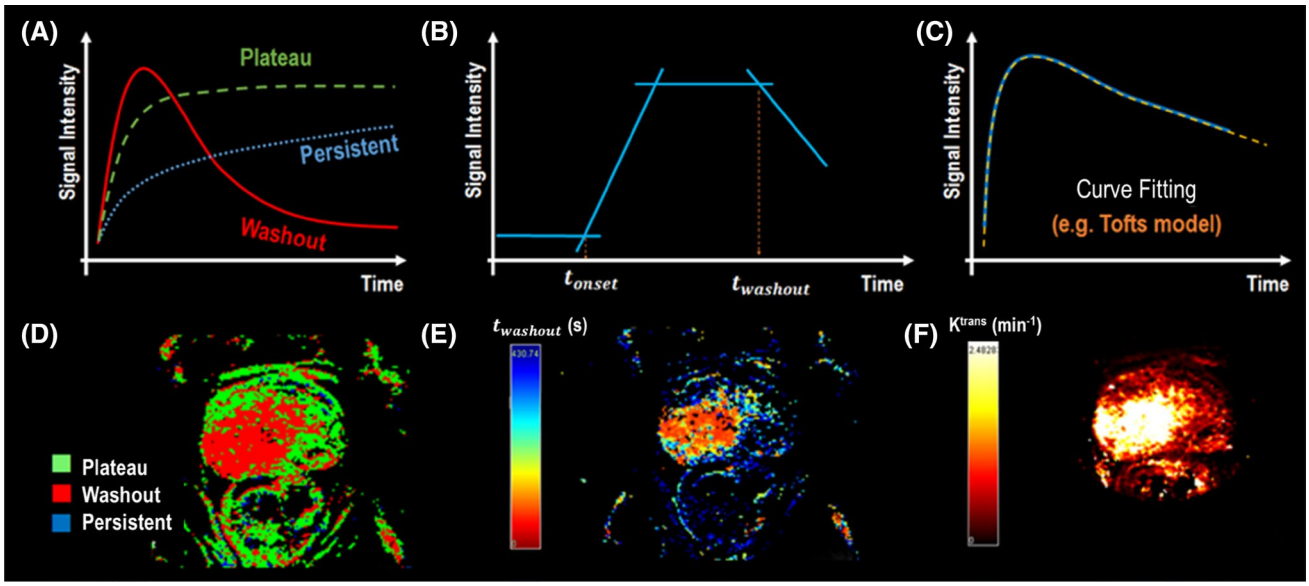

Fig. 4 Illustrations of three different approaches for analysing DCE-MRI data: **a** qualitative analysis, also known as the curve type analysis; **b** semi-quantitative analysis where descriptive features are computed from the dynamic curve (t_{onset} and $t_{washout}$ in this case); **c** quantitative analysis where a pharmacokinetic model (e.g. Tofts model) is used to fit the curve and compute pharmacokinetic maps. Three corresponding feature maps (**d**–**f**) from the same patient are shown, produced using the DYNAMIKA software (Image Analysis Group, London, UK): **d** a map indicating the curve type; **e** a $t_{washout}$ map and **f** a K^{trans} map fitted from the extended Tofts model. There is a Gleason score 4 + 3 = 7 tumour on the right side of the prostate

to an optional sequence and excluded it from the PI-RADS scoring system [9, 15].

Blood oxygen level dependent MRI

Haemoglobin has different magnetic properties depending on its oxygen-binding state [59]: oxy-haemoglobin is diamagnetic while deoxy-haemoglobin presents paramagnetic characteristics [60]. Blood oxygen level dependent (BOLD) MRI utilises the varying magnetic characteristics of haemoglobin to assess oxygenation status non-invasively. Although BOLD is not included in the PI-RADS recommended sequences, studies have reported the potential value of BOLD MRI in assessing tumour hypoxia [61] and for correlating with blood vessel maturity [62].

Current role of multiparametric MRI

The traditional role of mpMRI was confined to PCa staging, which was usually performed after the biopsy to assess the eligibility for different treatment options (e.g. active surveillance and radical prostatectomy) for an individual patient. However, due to the advanced imaging techniques, the role of mpMRI has expanded to include tumour detection, disease monitor during active surveillance and patient follow-up [63].

Detection of prostate cancer

Traditional detection of PCa using a transrectal ultrasound guided biopsy (TRUS) has revealed substantial limitations including a low detection rate (27–44%), over-diagnosis of clinically insignificant PCa while missing certain significant lesions, particularly in the anterior part of the prostate [64–66]. Performing mpMRI is now becoming clinical routine for patients suspected to have PCa and can be performed either before TRUS or after a negative TRUS result (ideally before). The lesion identified by mpMRI can also be targeted using either in-bore MRI-guided biopsy (MRI-GB) [67] or MRI-ultrasound (MRI-US) fusion biopsy [68]. Both MRI-GB and MRI-US fusion biopsy shows higher accuracy compared with using TRUS alone [10, 69–71], demonstrating the discriminative power of mpMRI in PCa detection. Moore et al. performed a systematic review comparing MRI-GB with standard TRUS on 555 cases and found that despite a similar detection rate of clinically significant PCa (43%), MRI-GB was more efficient with a third fewer men required for biopsy and a reduction of up to 10% of clinically

insignificant PCa detected [72]. A large study by Siddiqui et al., performed at the National Institutes of Health (NIH), compared TRUS and MRI-US fusion biopsy on 469 cases and found that the likelihood of missing a clinically significant PCa was much lower using MRI-US fusion biopsy than TRUS [73]. This agreed with another study involving 1448 patients which concluded that tumour detection was higher when using MRI-GB with a cancer detection rate of 70.1% (13.1% for TRUS) [74].

For patients who have been diagnosed with PCa, localisation and volume estimation of the tumour becomes critical for management and treatment selection. The use of mpMRI can facilitate accurate localisation of the tumour, especially anterior tumours that TRUS may miss [6]. In addition, mpMRI offers high accuracy in defining tumour volume, which has been shown to be a prognostic factor [75].

Assessment of aggressiveness and staging

Optimal clinical decision making requires estimations not only on tumour location and volume, but also on the aggressiveness and the overall stage of the disease. Previous studies have reported the correlation between ADC and Gleason scores [29, 76–81]. However, due to an inter-patient variability and an overlap of ADC values between different aggressiveness categories, no single cut-off values have been found to consistently distinguish between low-grade, intermediate-grade and high-grade tumour. Similar correlations were found between parameters from DCE-MRI and Gleason Score [82]. In addition, previous studies have investigated the combination of T2w MRI, DWI and DCE-MRI in determining tumour aggressiveness in PCa [78, 83, 84].

The ability to evaluate tumour volume, aggressiveness and the presence of extraprostatic extension makes mpMRI capable of PCa staging. Previous studies have compared mpMRI with traditional staging approaches, such as the Partin table, a staging system combining Gleason Score, prostate specific antigen (PSA) in the serum and clinical stage for predicting PCa locality. Augustin et al. carried out a two-step study by first validating the consistency of Partin tables using 2139 European men [85]. After the initial validation, Augustin et al. compared the performance of mpMRI and the Partin table in a prospective study with a conclusion that mpMRI showed a higher accuracy for staging localised PCa [86]. Similarly, Dickinson *et al*. reported a five-scale system for scoring significant disease (defined as Gleason Score $>=4+3=7$, lesions $>=0.5\ cm^3$) using mpMRI data: a score of 1 being least likely for clinically significant PCa and a score of 5 being most likely for significant disease [87]. Renard-Penna et al. [88] reported high accuracy using T2w imaging and DCE-MRI for PCa staging. This ability of mpMRI to estimate pathological stages aids the selection of treatment options. Tumours that extend beyond the prostate boundary (T3 stage) can be effectively identified using mpMRI [89], particularly on T2w images [8]. The presence of a T3 stage tumour is an indicator of metastatic disease, which is a critical factor in choosing between curative and palliative treatment, although patients with only minimal extraprostatic extension can still benefit from radical prostatectomy [90].

Treatment planning

The clinical details provided by mpMRI can be used to assist treatment planning. For patients with low-risk PCa, mpMRI can be used to evaluate the eligibility for active surveillance or to help with surgery and radiotherapy treatment planning [8]. If active surveillance is being considered using traditional detection procedures, mpMRI can be performed to detect any lesions missed by TRUS. For patients with intermediate-risk disease, mpMRI is useful in defining the locality of PCa and for detecting local invasion (e.g. extraprostatic extension) [8].

A thorough assessment of tumour location, volume, aggressiveness and the presence of EPE using mpMRI is useful for guiding focal therapy [91]. Currently, approaches for focal therapy are based on the index lesion hypothesis, so localisation of the index lesion is essential. Le et al. examined 122 men who had mpMRI scans prior to radical prostatectomy and found that mpMRI identified 80% of index tumours and achieved high accuracy for detecting high grade (Gleason score >6) and large volume (diameter >1 cm) tumours [92]. Similarly, Baco et al. [93] showed 95% of the index lesions identified on mpMRI agreed with histopathology from 135 radical prostatectomy specimens. Rud et al. [94] evaluated 199 men who underwent prostatectomy and mpMRI was able to detect the index tumour in 92% of the patients.

Despite the high detection rate of index lesions, there is a risk that mpMRI may miss secondary satellite lesions. However, Tan et al. [95] examined the characteristics of lesions missed by mpMRI from 122 cases and found that satellite lesions missed by mpMRI were significantly smaller and more likely to be low-grade tumour. In bio-focused radiotherapy, a low dose of radiation is applied to the non-tumour region and in this way any satellite lesions missed by mpMRI will still be treated with sufficient radiation dose. We anticipate this will improve tumour control and effectively address the controversy and reliance on the index lesion hypothesis, which is a major concern for current focal therapy approaches.

Prostate radiomics

Radiomics is the quantitative analysis of medical imaging data with the aim to extract clinical information which may have predictive value [96]. This is based on the hypothesis that a distinct tumour phenotypic differences can be captured by imaging features [97]. Therefore, the extraction and analysis of features from medical imaging data play an important role in radiomics. Previous studies have reported correlations between quantitative imaging features and treatment outcome or clinical measures (e.g. the presence of a tumour) [98]. The purpose is to identify potentially useful imaging features which can be used as indicators for pathogenic processes or response to therapeutic interventions, which are termed 'imaging biomarkers' [99]. Imaging biomarkers, along with other clinical information, are often used in combination to develop predictive models for clinical decision support systems. Hence data modelling techniques such as machine learning are often involved in radiomics studies.

The application of radiomics has shown advantages compared with conventional methods in cancer detection and characterisation. Firstly, as radiomics approaches are based on medical imaging such as MRI and CT (computed tomography), they are non-invasive and hence, minimise physical trauma to the patient and reduce limitations on the examination to be performed. Secondly, medical imaging enables the ability to capture the 2D and 3D representation of the tissue and more importantly, radiomics enables the quantification of intra-tumour heterogeneity by extracting a variety of features from imaging data [100]. This is particularly relevant as intra-tumour heterogeneity has been reported as an essential confounder influencing treatment efficacy and patient outcome [101], and conventional approaches in prostate cancer detection such as transrectal ultrasound (TRUS) biopsies typically lack the ability to provide a detailed spatial representation of tumour heterogeneity. Lastly, the implementation of radiomics is highly compatible with current routine patient care [102]. Commonly patients will have medical imaging scans during the disease diagnosis and treatment process. Hence minimal extra examination is required to perform radiomics analysis. In addition, historical medical imaging data archived in medical centres worldwide can function as a mineable resource. Retrospective studies can be performed, offering a high-throughput solution for knowledge discovery across the globe. This enables novel approaches for data mining using daily routine data, such as "rapid learning" [103]. In general, radiomics offers a cost-effective and high-throughput approach to medical imaging data analysis, which can lead to accurate tumour detection and aid personalised cancer treatment. Due to the versatility of mpMRI, it becomes the most commonly used medical imaging modality associated with prostate radiomics.

The major focus: computer-aided detection

Detection of prostate cancer in mpMRI data is the dominant focus of current prostate radiomics studies. The advent of radiomics has accelerated the process of predictive model development for indicating tumour location, known as computer-aided detection (CAD) [3, 4]. The intention of CAD systems is to advise and complement radiologists in PCa detection rather than replacing the radiologist [104]. Comprehensive reviews of CAD in prostate cancer have been provided by Wang et al. [3] and Lemaître et al. [4].

The development of a typical CAD model includes multiple steps [3, 4], as is shown in Fig. 5. After the initial mpMRI acquisition, images are pre-processed to reduce noise, correct for artefacts, remove image distortion and standardise signal intensity to reduce inter-patient variability. Prostate segmentation is then typically carried out, either manually or using automatic methods. The aim of segmentation is to define the boundaries of the prostate so that

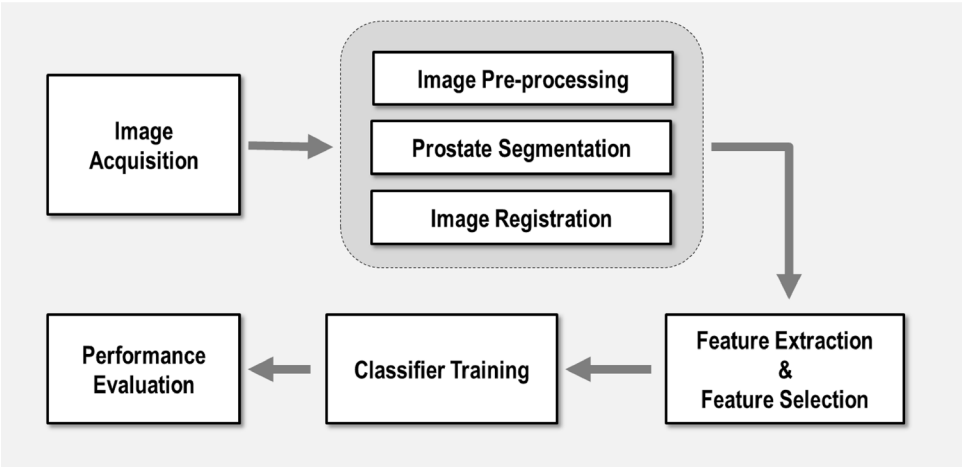

Fig. 5 Typical workflow of a CAD system

analysis can be focused on the specified volume. Following that, to bring imaging data into the same reference space, imaging data are often co-registered. Following this, various imaging processing methods can be applied to extract features (feature extraction) which can be further assessed as potential candidates for tumour location prediction. For studies using a large number of features, feature selection is often performed to select the most useful subset of features. Once features have been selected, they are used in training the predictive model, a classifier in this case. The performance of the classifier is evaluated using a different data subset, which gives an estimation of how well the classifier may perform in a similar clinical setting.

Prostate segmentation

MR images for the prostate typically contain neighbouring organs such as bladder and rectum. The aim of segmentation is to define the prostate boundary (optionally with the zones in the prostate) and exclude other nearby organs. Prostate segmentation can be performed using either manual or automated methods. The boundary of the prostate can be manually contoured on T2w images. This prostate contour can then be transferred onto other imaging modalities such as DWI and DCE-MRI, with the aid of image registration if required. Despite being time-consuming and labour intensive, manual segmentation is suitable when assessing a small patient cohort and has been used in a number of previous CAD studies [105–114]. To reduce the workload required by manual segmentation, automated prostate segmentation methods have been actively investigated. Commonly used methods include atlas-based segmentation [115–119] and model-based segmentation [120–123]. Recently, novel approaches for prostate segmentation have been developed, including methods using machine learning techniques such as deep neural networks (also generally known as 'deep learning') [124, 125]. However, the reliability and robustness of deep learning approaches in segmentation require further elucidation due to the limited interpretability of the model.

Image registration

In CAD, it is important to ensure the spatial correspondence of the prostate between different imaging modalities. The aim of image registration is to transform different datasets into the same coordinates. This is achieved by aligning one image (moving image) with a fixed image (reference image). Depending on the transformation applied, there are three types of image registration (rigid, affine and deformable registration). Rigid transformation accounts for translation and rotation, while affine transformation manages another two degrees of freedom, shearing and scaling. Complex local deformation can be handled using deformable registration, also known as elastic or non-rigid registration. Image registration has a vital role in CAD as displacement and deformation of the prostate may occur due to patient motion during the MRI acquisition. In addition, as a large number of CAD used ex vivo histology as ground truth, accurate alignment between in vivo mpMRI and ex vivo histology is crucial to develop a high-performance model.

Between in vivo MRI sequences Image registration between mpMRI sequences typically uses the T2w MRI as the reference image. All other functional images (and resulting parametric maps) are co-registered to the T2w image. The choice of optimal registration methods largely depends on the scanning protocol. In most cases, the deformation of the prostate between imaging sequences is minor and affine registration is sufficient. Hence a number of studies only applied affine registration for registering T2w images with DWI and /or DCE-MRI [113, 122, 126–129]. However, the likelihood of prostate deformation increases under certain circumstances, for example, if an endorectal coil or a protocol requiring a long scanning time is used. In such cases, the use of deformable registration may be necessary, such as studies reported by Giannini et al. [130] and Vos et al. [131].

Between in vivo MRI and ex vivo histology Histology obtained after prostatectomy is often used to provide the ground truth for CAD development. A number of studies have carried out image alignment visually, by directly comparing image slices on MRI with histology to determine slice correspondence [83, 105, 132, 133]. However, this method is highly subjective, assumes an MRI slice is cut in exactly the same orientation as histology and also can suffer from high variability between observers. To improve alignment accuracy, registration is preferred. The first approach is to co-register histology to mpMRI directly without any intermediate steps. Commandeur et al. [134] presented a method to reconstruct and register whole-mount histology with MRI data. Similar approaches have been applied by Xiao et al. [135], Chappelow et al. [136, 137], and Patel et al. [138].

In an attempt to improve registration accuracy, a number of studies have carried out ex vivo imaging of the prostate specimen and used these images during the registration process. For example, Park et al. [139] included ex vivo prostate scans, histology and block face photos of the specimen during their registration process. While Gibson et al. [140] marked the prostatectomy specimen with ten strand-shaped fiducial markers, which were used for an initial registration prior to a local refinement.

Some researchers have developed an apparatus to function as (1) a container for the prostate specimen so that ex vivo scans can be performed and (2) a guiding device for

prostate specimen sectioning to obtain slice correspondence between ex vivo scans and histology. The ex vivo scans of the prostate specimen function as an intermediate step for the registration between in vivo mpMRI scans and histology. Turkbey et al. [141] developed a customised patient-specific mould where structural information from in vivo imaging was used to inform 3D printing to fabricate the mould. The prostate specimen was placed in the mould for ex vivo imaging and sectioning purposes. A similar device has been presented by Bourne et al. [142], Shah et al. [143] and Priester et al. [144]. Despite the usability of 3D printed moulds, limitations in the assumptions exist as it is known the prostate specimen typically shrinks after surgery which may not be well supported by the mould design. Orczyk et al. [145] assessed the volume change of prostate following surgical resection and found that mean prostate volume was significant smaller for ex vivo (39.7 ± 18.6 cm^3) than in vivo (50.8 ± 26.8 cm^3). To address this issue, Reynolds et al. [146] developed a registration framework using agarose gel to fix the prostate specimen in a rectangular shaped sectioning box without utilising a customised mould. The agarose gel can surround the prostate specimen despite the shrinkage. A 3D deformable registration was then applied between in vivo and ex vivo MRI [146] to account for the shrinkage.

Feature extraction

Feature extraction is the process of computing additional features from mpMRI which can be used to improve a predictive model's discriminative power. In addition to commonly used features including edges features [108, 147–151], blob features [152–154] and statistical features (e.g. percentiles and moments) [83, 108, 109, 132, 133, 147, 154–156], texture features have gained significant popularity in the last decade. Texture features generally refer to features that capture the complex visual pattern and spatial relationship between neighbouring voxels. Haralick's texture features are the most widely reported, which are based on the gray-level co-occurrence matrix (GLCM) [157, 158]. A GLCM defines the pattern of an image subregion by summarising the appearance of voxel pairs with a specific discretised grey-level value in a specified direction. Similar texture features have been developed using the gray-level run length matrix (GLRLM) [159] and the gray-level size zone matrix (GLSZM) [160]. A GLRLM summarises the frequency of continuous voxels that have the same discretised grey level value in a given direction. The length of the continuous section defines a "run length". In a GLSZM, pixels are connected if they have the same discretised grey level value and connected pixels form zones. A GLSZM counts the occurrence of zones with a specific grey level value and with a specific size. Both GLRLM and GLSZM apply different approaches to quantifying statistical properties of an image subregion.

Recent studies have revealed the heterogeneous nature of tumours, which presents to be a major challenge in cancer treatment. Texture features can be used to assess tumour heterogeneity. Combined with the 3D nature of imaging, this enables quantitative assessment of tumour heterogeneity and evaluation of new biomarkers. Kuess et al. [161] assessed the association between prostate pathology and texture features from mpMRI and presented a CAD model using orthogonal partial least squares discriminant analysis. Chung et al. [162] used high-volume radiomics features extracted from mpMRI for PCa detection. In another study by Chung et al. [163], a novel texture feature discovery framework was proposed to address the limitation that most texture features were manually defined. The authors evaluated the performance of features identified by the proposed method and demonstrated improved performance (an accuracy of 0.74, compared with manual-defined features: 0.58 and 0.67) [163]. Ginsburg et al. [164] evaluated the performance of texture features in CAD in both PZ and TZ and found that zone-specific models outperformed zone-ignorant models. Khalvati et al. [164] designed a radiomics-based automated method for PCA detection using an SVM model.

Feature selection

Feature selection involves selecting a portion of the most important features for model training. Reasons for carrying out feature selection are fourfold. First, a large number of features can cause some machine learning algorithm to fail due to the high dimensionality of the feature space. This is known as the "curse of dimensionality", and happens because as the volume of feature space increases, data becomes sparser and the discriminative power decreases. Second, a reduced number of features can enhance model generalisation by reducing the chance of overfitting. Third, information redundancy and high correlation between features (collinearity) can cause model instability. Similarly, features can be correlated with linear combinations of the remaining features (multicollinearity), which is even more difficult to detect than collinearity. Fourth, choosing a feature subset improves the interpretability of the model and shortens the training time.

There are generally two categories of feature selection methods. The first approach uses statistical measures to filter available features. This approach computes a statistical parameter (e.g. p value of a statistical test) for each feature and applies a threshold to select a feature subset. Niaf et al. [108, 109] applied independent two-sample t-test for each feature and used the associated p value to rank the features based on significant level. Vos et al. [152] applied a similar approach by using the Fisher discriminant ratio for feature

ranking. A threshold was then set to select features with a large Fisher discriminant ratio [152]. Most previous radiomics studies mainly focused on reducing the feature number, and few studies considered issues like information redundancy such as collinearity. Manual removal of data is an effective way to address collinearity if a high correlation between two features is observed. Iyama et al. [165] reported a logistic regression model for TZ PCa, where minimum ADC was manually excluded from the model due to its collinearity with mean ADC. Similarly, mutual information can be used as a metric to assess redundancy. Peng et al. [165] proposed a method which combined maximal relevance and minimum redundancy (mRMR) for feature selection. A two-stage algorithm was developed by combining mRMR with other sophisticated feature selectors, which allowed selection of high-performance features at low cost [165]. Methods based on mRMR have been adopted in a number of CAD studies [108, 109, 166–168].

The second approach for feature selection utilises dimension reduction techniques, which projects data from a high dimensional space to a lower dimensional space. New features are then constructed using combinations of original features. This approach is best suited for handling information redundancy. Principal component analysis (PCA) is the most commonly used technique for dimension reduction in CAD. PCA linearly decomposes the original features and forms a new set of variables, called principal components. A major advantage is that principal components are orthogonal so that no collinearity or multicollinearity presents between them. In addition, there is a high flexibility in choosing the number of principal components, which are typically ranked by the variance they carry. PCA has been used in multiple CAD studies for dimension reduction [169–171]. Locally linear embedding (LLE) is another dimension reduction method. Unlike PCA which is a linear method, the new variables formed by LLE are non-linear combinations of the original features. Tiwari et al. [171] applied a modified version of LLE with bagging methods. Other non-linear dimension reduction methods include Laplacian eigenmaps, also known as spectral clustering. Viswanath et al. [151] and Tiwari et al. [148, 170, 172] applied spectral clustering to construct a new set of features. Although dimension reduction methods have an advantage in handling information redundancy, it comes with the price of losing feature interpretability. In CAD, features based on mpMRI typically correspond to different biological properties, such as ADC. Hence combining one property with another can mean it loses its biological meaning, which may pose a barrier when explaining the model.

Classifier training

After feature selection is completed, the next step in prostate CAD involves training a classifier. To be able to evaluate model performance, a portion of the imaging data available is typically reserved and will not be used in the training process. One approach is to partition the data into training data and test data (or validation data), using the training data for classifier training and the test data for performance evaluation. Cross validation (CV) is an iterative approach used which is based on data partitioning. There are two types of CV, namely k-fold CV and leave-one-out CV (LOOCV). In k-fold CV, the whole dataset is partitioned into k trunks. One trunk will be used as test data with the remaining (k-1) trunks used as training data. This process is repeated k times until each trunk has been used as the test data. LOOCV is a special case of k-fold CV, where k is equal to the total number of samples and each sample is used as the test data at each iteration. Both k-fold CV and LOOCV are widely used in CAD studies.

After defining the training and test framework, data is passed into a machine learning algorithm to build the classifier. A number of different algorithms are available for this, and the following section introduces three of the commonly used algorithms: logistic regression, support vector machines and Random Forest.

Logistic regression Logistic regression (LoR) is a probabilistic method for classification, despite the presence of 'regression' in its name. It belongs to a larger family called generalised linear models. LoR uses a logistic function (or sigmoid function) as a link function to map the linear combination of features to the interval between 0 and 1. In CAD, the output of LoR can be interpreted as the probability that a voxel or ROI is a tumour. The expression of the logistic function s is shown in Eq. (2).

$$s(\boldsymbol{X}) = \frac{1}{1 + \exp(-\boldsymbol{X})} \tag{2}$$

The original LoR is used to model binary outputs which follow a binomial distribution. This is the major difference from other regression methods, with outputs that generally follow a Gaussian distribution. Generalisation has been made to extend binary LoR to multiclass classification and to ordinal outputs. For a LoR parametrised by θ with training data $(\boldsymbol{X}, y)$, the likelihood function L can be expressed using Eq. (3).

$$\begin{aligned} L(\theta|\boldsymbol{X}) &= \prod_i \Pr(y_i|\boldsymbol{X}_i, \theta) \\ &= \prod_i s(\boldsymbol{X})^{y_i} \cdot (1 - s(\boldsymbol{X}))^{1-y_i}. \end{aligned} \tag{3}$$

Coefficients of LoR (θ) can be estimated by *maximising the likelihood function L* using numerical optimisation.

Niu et al. [173] developed a LoR model for high-grade PCa. Using a cut-off on the LoR model output, the sensitivity and specificity were 87.3% and 78.4%, respectively [173]. Langer et al. [174] applied a stepwise LoR model for CAD using mpMRI and achieved an optimal AUC of 0.706. Dikaios et al. [175] developed a LoR model for classifying PCa within the TZ and found that LoR models can improve classification of PI-RADS score three lesions similar to experienced radiologists. In another study, Dikaios et al. [176] investigated the interchange usability of LoR models between PZ and TZ and concluded that LoR models dependent on DCE-MRI alone are not interchangeable between zones. However, LoR models built on T2 or ADC are robust for cross-zonal application [176], which demonstrated the potential value of zone-independent models.

Support vector machines Support vector machines (SVMs) are binary classification method which has gained substantial popularity recently for machine learning applications. It is also the most commonly used algorithm in CAD studies. SVM represents an algorithm family called sparse kernel methods. The keywords 'sparse' and 'kernel' define two characteristics of SVM. First, SVM determines hyper-planes as decision boundaries (support vectors) in the feature space by maximising the margin between two groups. Hence, the decision boundaries are only dependent on samples near the support vectors, which is typically a small portion of the dataset ("sparse" property). In addition, for complex patterns where a linear separation cannot be found, data can be mapped to higher dimensional spaces for separation, known as kernel methods. This results in a non-linear decision boundary when mapped back to the original low dimensional space. Commonly used kernels include the Gaussian kernel (also known as the radial basis function) and the polynomial kernel. One advantage of SVM is that high dimensional mapping can be computed implicitly using the kernel trick, which tremendously reduces the computational load and enables large-scale model training. Similar to LoR, there are generalisations to extend binary SVM to multiclass SVM and one-class SVM. Due to the nature of CAD where only two classes are involved, binary SVM is often sufficient.

A large number of other studies used SVM to develop CAD applications. Vos et al. [114] developed a novel CAD framework for PZ PCa using DCE-MRI. An SVM model was trained using a feature set combining pharmacokinetic parameters and T1 estimates, with an accuracy of 0.83. Similarly, Shah et al. [177] presented a decision support system for PCa detection using mpMRI and compared the performance of SVM models before and after parameter optimisation. The SVM achieved a Kappa coefficient of 71% prior to optimisation, while this number increased to 80% after optimisation. This demonstrates the necessity of parameter optimisation to maximise the efficacy of SVM models.

Random forest Random Forest is an ensemble classification method based on the classification or regression tree (CART). A large number of CART are built which forms an ensemble of tree models. Majority vote can be performed based on the tree ensemble. This can result in either a binary output (the label for the majority trees) or a probability (fraction of trees with a specific label). Each tree is constructed using a subset of samples and a portion of the features to minimise overfitting. One advantage of Random Forest is the use of ensemble learning, which combines a group of weak learners into a strong learner. It has been shown that ensemble methods improve prediction performance compared to individual members. In addition, variable importance can be obtained by permuting the features and measure performance loss. However, the ensemble approach has limitation such as model interpretability. Unlike a single CART where the explanation can be found at each split, the effect of a specific feature is hard to define in a Random Forest. Nonetheless, this does not prevent Random Forest from being a useful non-parametric method.

Previous studies have shown that Random Forest generally has high performance. Lay et al. [178] applied a Random Forest model with instance weighting to detect PCa using T2w imaging and DWI and compared its performance with an SVM model. The Random Forest yielded an AUC of 0.93, which outperformed the SVM model (AUC = 0.86) on the same test data. Similarly, Qian et al. [179] proposed a novel CAD framework to identify PCa regions using Random Forest and auto-context model. The proposed method outperformed conventional methods such as adaptive boosting. In another study by Trigui et al. [179], the authors compared the error rate of a Random Forest model with an SVM model in classifying tissues into three classes (healthy, benign and pathologic). The Random forest had an error rate of 24.6%, which was lower than that of the SVM model (26.0%).

Performance evaluation

Various metrics are used to evaluate model performance, which is carried out on the testing data or using CV techniques. The first approach is to compute the ratio of voxels (or ROIs) that have been correctly classified, as is defined by accuracy. Accuracy has been used in a number of studies [105, 106, 169, 180, 181]. However, for imbalanced data model assessment accuracy can be highly biased and it is more suitable to assess model performance using sensitivity and specificity which has been done in multiple CAD studies [83, 105, 110, 111, 123, 130, 151, 170, 171, 180,

182–184]. For classification models that generate a continuous output (e.g. a probability map instead of a binary mask), the receiver operating characteristic (ROC) curve provides an intuitive way to assess the performance [185]. The area under the curve (AUC) of the ROC curve offers a quantitative measure for model performance, which has been used by the majority of previous CAD studies in performance assessment [108, 109, 127, 130, 148, 149, 183, 186–188]. An extension of the ROC curves results in what is termed the free receiver operative characteristic (FROC) curve, which allows for multiple responses (rather than binary responses) [152, 154, 155]. Another similar approach for model evaluation is based on precision and recall. Equivalent to AUC in ROC curves, F-measure offers a quantitative measure combining precision and recall. However, few study have used F-measure to report model performance [177]).

In one review by Wang et al. [3], the AUC of ROC curves ranges between 0.77 and 0.96. This agreed with another

Table 1 A brief summary of methods in prostate radiomics

Tasks	Methods	Advantages[a]	Limitations[a]
Segmentation	Manual	Directly performable No additional setup requirements	Time consuming and labour intensive Human expertise required
	Automatic	Fast to perform Fully automatable Minimal human interventions	Requires validation of the methodology Requires a high quality set of pre-segmented images for atlas-based segmentation
Image registration	Non-deformable	Fast to perform Accounts for translation, rotation, shearing and scaling	Unable to account for irregular deformations
	Deformable	Accounts for deformations on top of non-deformable registration methods	Computationally intensive May lead to unrealistic results
Feature extraction	Edges, blobs and statistical features	Detects low-level characteristics of an ROI Have a physical or statistical meaning Widely implemented in software packages	Difficult to describe inter-voxel spatial relationships Difficult to quantify region heterogeneities
	Texture features	Detect high-level characteristics of an ROI Able to describe spatial relationships between voxels Quantitatively assess the heterogeneity of an ROI	Not widely implemented in software packages Collinearity exists between features Not all have a clearly-defined meaning
Feature selection	Filtering	Can be applied in a step-wise approach Various filtering metrics can be applied The interpretation of a feature is retained	Computationally intensive for a large feature set In some cases, the result is sensitive to the sequential order
	Dimension reduction	Output features can be ranked based on the information value Output features can have favourable properties (e.g. orthogonality) Works efficiently for large feature sets	The interpretability of the output is compromised Results are sensitive to scaling
Classifier training	Logistic regression	The output has probabilistic interpretations Weights are related to feature importance Can be used for multi-class learning No hyper-parameters to fine tune	May be insufficient to handle complex patterns
	Support vector machine	Can be used with kernel methods Different sub-types available for one-class, binary and multi-class learning Not reliant on the entire dataset (sparse method)	May overfit the data with complex kernels Requires hyper-parameter tuning Difficult for model interpretation
	Random forest	Applies ensemble learning to reduce the prediction bias Applies bagging to reduce over-fitting Provides the relative feature importance	Requires hyper-parameter tuning The overall model is hard to interpret

[a]For general guidance only, the advantages and limitations are subject to specific cases

review by Lemaître et al. that the range of AUC is between 0.71 and 0.97 with 1.5 T machines and between 0.77 and 0.95 for 3.0 T machines [4]. In addition, the sensitivity ranges from 0.74 to 1.0 and the specificity ranges from 0.43 to 0.93 for 1.5 T machine and for 3.0 T MRI, these ranges are 0.60–0.90 and 0.66–0.99, respectively [4]. However, comparisons between different studies should be carried out with caution due to the high variability in experimental setups such as MRI magnetic field, patient cohort size, registration method and machine learning algorithm.

The advantages and limitations of different methods are shown in Table 1.

Future directions of prostate radiomics

Prostate radiomics is a rapidly developing field where early studies initially focused on tumour localisation. An overview of prostate radiomics studies enables identification of the development pattern and future directions of this subject (Fig. 6). The following section discusses three key aspects for the direction of prostate radiomics development in three aspects: imaging features, data analysis and biological correspondence.

The application of high-level features

Imaging features function as essential components in radiomics approaches as they provide a rich source of potentially useful biomarkers. From the perspective of machine learning, the predictive power of a model relies on the proper use of suitable features. Previous studies have identified a variety of imaging features in prostate radiomics. Edge features are among the most commonly used features. Edges are defined as the boundary between two image regions which have a strong gradient of the signal intensity. In prostate mpMRI, this could correspond to the boundaries of different zones or PCa lesions. Convolutional filters for edge detection include the Sobel operator, Canny operator, Prewitt operator, Kirsch operator and Gabor operator, which have had a wide application in prostate radiomics, particularly in CAD development [108, 147–151]. Blob detection is another technique widely used. A blob is a region that differs from the surrounding environment in terms of signal intensity. PCa tends to have focal blob-like properties in DWI and DCE-MRI [152]. This characteristic has been utilised in multiple previous studies for defining tumour volumes from mpMRI [152–154]. In addition, the application of wavelet features and statistical features such as percentile values and statistical moments have also been widely reported [83, 108, 109, 132, 133, 147, 154–156, 189].

Despite the widespread use of various imaging features, recent studies have appreciated an increasing use of texture features in detecting and biologically characterising prostate cancer. The increasing use of texture features is driven by multiple factors. First, there exists a number of texture features previously defined by computer vision methods. Second and more importantly, texture features are able to assess tumour heterogeneity, which provides an approach to correlate imaging data with tissue phenotype. In prostate radiomics, Haralick's texture features are the most widely

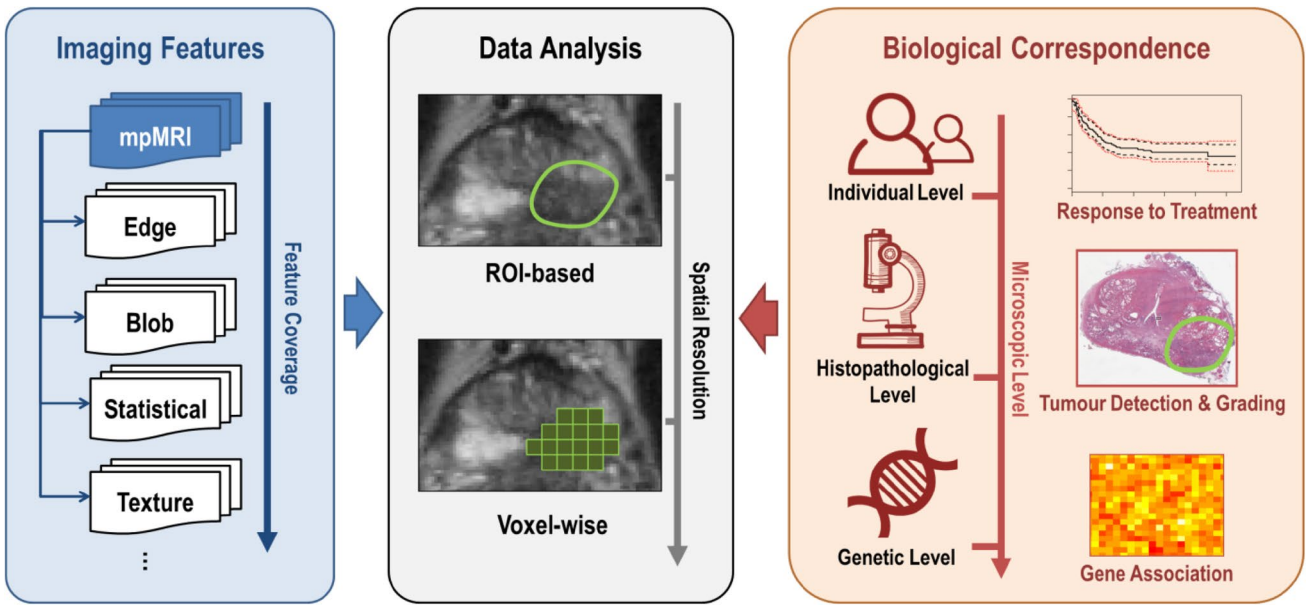

Fig. 6 Three different aspects of prostate radiomics development: the use of texture features, development of voxel-wise predictive models and a migration towards analysis at the microscopic level

reported texture features, which are based on the gray-level co-occurrence matrix (GLCM) [157, 158]. A GLCM defines the pattern of an image region by counting the occurrence of voxel pairs with a specific discretised grey level value in a given direction. The application of Haralick's texture features in defining prostate tumour has been demonstrated by a number of studies [108, 122, 128, 147, 154, 161, 166, 190, 191]. In addition, there is accumulating evidence that Haralick's texture features correlate with tumour biological characteristics, such as tumour aggressiveness [192–194]. This suggests a broader application of texture features for determining the biological properties of the tumour.

While texture features have gained substantial popularity, the majority of previous studies have only investigated GLCM-based features, such as Haralick's texture features. However, there are other types of texture features, including those based on the grey-level run length matrix (GLRLM) [159], the gray-level size zone matrix (GLSZM) [195], the neighbouring gray-level dependence matrix (NGLDM) [196], the neighbourhood gray-tone difference matrix (NGTDM) [197] and the gray-level distance zone matrix (GLDZM) [195]. Hence a migration from the well-investigated Haralick's texture features to these non-GLCM features is not unexpected. Recent studies after 2014 have demonstrated an increasing use of non-GLCM features in defining prostate tumour location [190, 198, 199], and it is anticipated that future studies will expand their use in predicting tumour biological characteristics.

From region-based to voxel-based approaches

In radiomics studies, analysis can be performed using either a region of interest (ROI) based approach or a voxel-wise approach. The choice of whether to use an ROI-based or voxel-wise approach generally depends on the quality of the image registration techniques applied. This is because the ground truth in prostate radiomics studies is often obtained from histology to achieve a high spatial accuracy. Hence a high-quality co-registration between in vivo mpMRI data and ground truth histology is necessary for voxel-wise analyses.

A number of studies have reported multiple devices to support ex vivo scans and sectioning of prostate specimens. Turkbey et al. [141] developed a customised patient-specific mould where structural information from in vivo imaging was used to inform 3D printing to fabricate the mould. The ex vivo specimen was then placed in the mould during ex vivo scans. Similar devices have been proposed by Bourne et al. [142] and Priester et al. [144]. However, the performance of 3D printed moulds is limited as the prostate specimen shrinks after surgery by an average of 10% and may not be well supported by the mould design [145]. To address this issue, the registration framework developed by Reynolds *et al*. used agarose gel to fix the prostate specimen in a rectangular shaped sectioning box without utilising a customised mould. The shrinkage was then accounted for by applying 3D deformable registration between in vivo and ex vivo MRI [146].

Due to advances in image registration techniques, there appears to be a move from using ROI-based approaches to performing voxel-wise analyses. Prior to 2014, prostate radiomics studies were often carried out using simple registration methods or without image registration [3, 105, 132–134. In a review of CAD model development, seven out of 16 studies before 2014 used manual ROI delineations to generate candidate lesions [3]. Although there is no systematic survey on the use of ROI-based approaches in post-2014 prostate radiomics studies, a number of studies have since benefited from improved co-registration methods and performed voxel-wise analyses [200–203].

Correlating imaging data with underlying biology

The application of radiomics in prostate cancer has spanned from the macroscopic to the microscopic level in terms of its biological correspondence. The highest level is on individual patients and the corresponding analysis is typically on predicting treatment outcome. Previous studies have investigated the value of mpMRI in associating biochemical recurrence (BCR) following radiotherapy [204]. Gnep et al. investigated the association between Haralick's texture features on mpMRI and BCR after radiotherapy. The results indicated that three texture features calculated from T2w images and ADC maps, along with tumour volume and tumour area, achieved significant correlations with BCR (C-index: 0.76 to 0.82, $p < 0.05$) [205]. Ginsburg et al. extended this approach further by developing a multivariate logistic regression model using T2w texture features for predicting BCR following radiotherapy. The model achieved an AUC of 0.83 [206]. Similar studies have been performed to investigate the BCR following other primary treatment options. Park et al. retrospectively assess the performance of ADC for predicting BCR after surgery and found that ADC could be used as an independent predictor (AUC = 0.76) [207]. Current prognostic studies using radiomics to date have mainly focused on lung cancer, and the number of studies in prostate cancer is relatively small. However, most radiomics techniques developed in lung cancer are cancer-unspecific so they can be applied in prostate cancer radiomics studies in the future.

The second category of radiomics in prostate cancer falls into the histopathological level. Whilst tumour detection has been the dominant application to-date, recent studies have moved towards the assessment of tumour biology, such as tumour aggressiveness. Correlation analyses have identified a consistent negative correlation between apparent diffusion coefficient (ADC) values and tumour aggressiveness,

measured by the Gleason Score (GS) [80, 208, 209]. The additional use of texture features has further facilitated the development of predictive models for tumour aggressiveness [193, 194, 210–212]. A few T2w texture features have been proposed as imaging biomarkers for tumour aggressiveness [194, 212]. Investigations have also been performed on prostate cellularity, and multiple investigators have consistently found negative correlations between ADC and cell density [25, 213, 214]. Exploratory investigations have also been carried out for assessing hypoxia status. Hoskin et al. investigated the correlation between R2* maps from blood oxygen level dependent (BOLD) MRI with immunohistochemistry (IHC) staining on pimonidazole (an exogenous marker) with the conclusion that R2* had a high sensitivity but low specificity for defining tumour hypoxia [61]. However, most analyses of tumour biology remain at the correlation stage, and predictive models are only available for tumour aggressiveness.

Moving to the microscopic level, the integration of radiomics and genomics has formed "radiogenomics" which aims to identify the correlation between quantitative imaging features and gene expression levels [215, 216]. This is the third category in prostate cancer radiomics, and despite being in its infancy, radiogenomics has shown its value in a number of preliminary studies. First, both the mpMRI and genetic information appear to reflect the varying pathological status of the tissue. For example, Jamshidi et al. [217] assessed mpMRI and the underlying genomic variations of normal and cancerous regions in the prostate. Both the imaging and genomic data showed a continuum of mutations across regions between high-grade tumours and normal tissues. In addition, an association between imaging features and genetic variations was found. Stoyanova et al. [218] investigated the correlation between 49 radiomic features with three clinically available gene sets associated with adverse outcome using prostate biopsy samples. The results found significant correlations between the selected genes and imaging features. In another study, Stoyanova et al. [219] reported 22 "decipher genes" which showed great potential for defining the risk group of individual patients. Other studies have applied radiogenomic approaches for correlating hypoxia [220] and PTEN expression levels [221], a prognostic indicator for biochemical recurrence. These findings show the potential of radiogenomics approaches for assessing tumour characteristics at the genetic level, which could be used in personalised treatment.

In summary, current prostate radiomics studies focus primarily on the histopathological level, with large numbers of applications in tumour detection and aggressiveness stratification, while predictive models remain to be developed for other tumour biological characteristics. At the genetic level, initial radiogenomics studies have shown promising results in prostate cancer and hence a fast uptake and growth of this technique are expected.

Potential issues

There are some data-specific issues and pitfalls which can occur in a radiomics study. These issues can lead to poor predictive modelling performance or biased interpretation of the data. Identifying these issues at the early stage of the study is able to minimise their potential impact and maximize the value of available data. Two of these issues are collinearity and data imbalance as discussed in the following sections.

Collinearity

Typically, the number of features used in radiomics studies range from tens to hundreds. Hence it is highly likely that two features will be correlated, which is defined as collinearity. Collinearity can be detected by computing the pairwise correlation coefficients of each feature pair. However, when a feature is correlated with the combination of two or more other features (referred as multicollinearity), it is much harder to detect. Typically, multicollinearity is examined using the variance inflation factor (VIF). Collinearity or multicollinearity can cause instability in a model [222]. This is particularly true in the case of linear models. This is because the inter-correlation between features can affect the coefficient estimation for each variable. Hence the magnitude of the coefficients may not accurately reflect feature importance, which poses a barrier in model interpretation. In addition, the model can also suffer from high variance due to the instability of coefficients associated with intercorrelated features. Hence, performing feature selection is crucial in radiomics studies to account for collinearity. Multiple options are available to cope with collinearity or multicollinearity, such as VIF regression or principal component analysis [223].

Data imbalance

Data imbalance refers to when there is a substantial difference in class size within the available data. Issues may arise when this occurs because most standard classification algorithms aim to optimise the overall performance of all samples. The consequence is the model may favour the majority of the class and result in poor accuracy in the minority class. For example, ROIs extracted from large prostate tumours can outnumber that from small tumours, which can result in a class imbalance towards the larger tumours. In general, data imbalance is commonly found in predictive radiomics studies. Different algorithms show varying tolerances when dealing with imbalanced classes. Therefore choosing

an appropriate algorithm which is robust to skewed classes is a simple approach to account for data imbalance. Crone and Finlay [224] examined the effect of data imbalance using four typical algorithms: logistic regression, linear discriminant analysis (LDA), decision trees and neural networks. The authors found that logistic regression was the most robust algorithm and decision trees were the least robust method. LDA and neural networks showed an intermediate level of sensitivity for data imbalance. Alternatively, sampling methods can be applied to generate a class-balanced dataset for training purposes. For example, the Synthetic Minority Oversampling Technique (SMOTE) is one such sampling method [225]. SMOTE synthesises new minority class samples by interpolating between existing minority samples which are close in the feature space. SMOTE has been applied as a data-based approach for imbalanced data in a number of prostate radiomics studies [192, 226].

Conclusions

The development of mpMRI has significantly expanded its role in prostate cancer detection, characterisation and patient management. To maximise the efficiency of extracting useful information from mpMRI, radiomics provides a toolbox for quantitative analysis. While the majority of prostate radiomics studies focused on tumour detection and localisation, recent studies have demonstrated the use of mpMRI in defining tumour biological properties such as tumour aggressiveness and the presence of hypoxia. There is also a trend in moving towards the microscopic level. This resulted in new paradigms such as radiogenomics where medical imaging and cancer genomics meet. These developments facilitate the discovery of imaging biomarkers which may have predictive power for treatment response and patient survival. In addition, the tumour location and characteristics estimated from mpMRI offer an opportunity to retrieve patient-specific profiles of the disease for personalised treatment. Such estimations can be used in pre-validated radiobiological models to individualise treatment planning. This will be an advancement compared with the traditional non-discriminatory treatment approach.

Acknowledgements The authors would like to acknowledge Peter MacCallum Cancer Centre, The University of Melbourne and Cancer Therapeutics CRC for providing the resources to perform the literature survey. The authors would also like to show their gratitude to Courtney Savill and Lauren Caspersz for their contributions in data collection.

Funding This study is supported by PdCCRS grant 628592 with funding partners: Prostate Cancer Foundation of Australia, and the Radiation Oncology Section of the Australian Government of Health and Aging and Cancer Australia. Yu Sun is funded by the Melbourne International Research Scholarship, a Movember Young Investigator Grant through Prostate Cancer Foundation of Australia (PCFA) and Cancer Therapeutics Top-up Funding. Hayley Reynolds is funded by a Movember Young Investigator Grant through PCFA's Research Program.

Compliance with ethical standards

Conflict of interest The authors declare that they have no conflicts of interest.

Ethical Approval This article does not directly involve human participants or animals, but contains example prostate MR images from another study approved by Human Research Ethics Committee (HREC).

Informed Consent Informed consent was obtained from all individual participants.

References

1. Johnson LM, Turkbey B, Figg WD, Choyke PL (2014) Multiparametric MRI in prostate cancer management. Nat Rev Clin Oncol 11(6):346–353
2. Steenbergen P, Haustermans K, Lerut E, Oyen R, De Wever L, Van den Bergh L, Kerkmeijer LGW, Pameijer Fa, Veldhuis WB, van der Voort van Zyp JRN, Pos FJ, Heijmink SW, Kalisvaart R, Teertstra HJ, Dinh CV, Ghobadi G, van der Heide UA (2015) Prostate tumor delineation using multiparametric magnetic resonance imaging: inter-observer variability and pathology validation. Radiother Oncol 15:186–190
3. Wang S, Burtt K, Turkbey B, Choyke P, Summers RM (2014) Computer aided-diagnosis of prostate cancer on multiparametric MRI: a technical review of current research. BioMed Res Int 2014:11
4. Lemaître G, Martí R, Freixenet J, Vilanova JC, Walker PM, Meriaudeau F (2015) Computer-aided detection and diagnosis for prostate cancer based on mono and multi-parametric mri: a review. Comput Biol Med 60:8–31
5. Thompson J, Lawrentschuk N, Frydenberg M, Thompson L, Stricker P (2013) The role of magnetic resonance imaging in the diagnosis and management of prostate cancer. BJU Int 112(S2):6–20
6. Gupta RT, Kauffman CR, Polascik TJ, Taneja SS, Rosenkrantz AB (2013) The state of prostate MRI in 2013. Oncology 27(4):262
7. Pedler K, Kitzing YX, Varol C, Arianayagam M (2015) The current status of MRI in prostate cancer. Aust Family Physician 44(4):225–230
8. Barentsz JO, Richenberg J, Clements R, Choyke P, Verma S, Villeirs G, Rouviere O, Logager V, Fütterer JJ (2012) ESUR prostate MR guidelines 2012. Eur Radiol 22(4):746–757
9. Weinreb JC, Barentsz JO, Choyke PL, Cornud F, Haider MA, Macura KJ, Margolis D, Schnall MD, Shtern F,Tempany CM, Thoeny HC, Verma S (2016) PI-RADS Prostate Imaging - Reporting and Data System: 2015, Version 2. Eur Urol 69(1):16–40
10. Villers A, Puech P, Mouton D, Leroy X, Ballereau C, Lemaitre L (2006) Dynamic contrast enhanced, pelvic phased array magnetic resonance imaging of localized prostate cancer for predicting tumor volume: correlation with radical prostatectomy findings. J Urol 176(6):2432–2437

11. Mueller-Lisse U, Mueller-Lisse U, Scheidler J, Klein G, Reiser M (2005) Reproducibility of image interpretation in MRI of the prostate: application of the sextant framework by two different radiologists. Eur Radiol 15(9):1826–1833
12. Nogueira L, Wang L, Fine SW, Pinochet R, Kurta JM, Katz D, Savage CJ, Cronin AM, Hricak H, Scardino PT et al (2010) Focal treatment or observation of prostate cancer: pretreatment accuracy of transrectal ultrasound biopsy and T2-weighted MRI. Urology 75(2):472–477
13. Arumainayagam N, Kumaar S, Ahmed HU, Moore CM, Payne H, Freeman A, Allen C, Kirkham A, Emberton M (2010) Accuracy of multiparametric magnetic resonance imaging in detecting recurrent prostate cancer after radiotherapy. BJU Int 106(7):991–997
14. Villers A, Lemaitre L, Haffner J, Puech P (2009) Current status of MRI for the diagnosis, staging and prognosis of prostate cancer: implications for focal therapy and active surveillance. Curr Opin Urol 19(3):274–282
15. Weinreb JC, Barentsz JO, Choyke PL, Cornud F, Haider MA, Macura KJ, Margolis D, Schnall MD, Shtern F, Tempany CM, Thoeny HC, Verma S (2015) PI-RADS prostate imaging—reporting and data system: 2015, version 2. Eur Urol 69(1):16–40
16. Akin O, Sala E, Moskowitz CS, Kuroiwa K, Ishill NM, Pucar D, Scardino PT, Hricak H (2006) Transition zone prostate cancers: features, detection, localization, and staging at endorectal mr imaging. Radiology 239(3):784–792
17. Wang L, Mazaheri Y, Zhang J, Ishill NM, Kuroiwa K, Hricak H (2008) Assessment of biologic aggressiveness of prostate cancer: correlation of mr signal intensity with Gleason grade after radical prostatectomy. Radiology 246(1):168–176
18. Liu W, Turkbey B, Sénégas J, Remmele S, Xu S, Kruecker J, Bernardo M, Wood BJ, Pinto PA, Choyke PL (2011) Accelerated T2 mapping for characterization of prostate cancer. Magn Reson Med 65(5):1400–1406
19. Liney GP, Lowry M, Turnbull LW, Manton DJ, Knowles AJ, Blackband SJ, Horsman A (1996) Proton MR T2 maps correlate with the citrate concentration in the prostate. NMR Biomed 9(2):59–64
20. Gibbs P, Tozer DJ, Liney GP, Turnbull LW (2001) Comparison of quantitative T2 mapping and diffusion-weighted imaging in the normal and pathologic prostate. Magn Reson Med 46(6):1054–1058
21. Kirkham APS, Emberton M, Allen C (2006) How good is MRI at detecting and characterising cancer within the prostate? Eur Urol 50(6):1163–1175
22. Hoeks CMA, Barentsz JO, Hambrock T, Yakar D, Somford DM, Heijmink SW, Scheenen TWJ, Vos PC, Huisman H, van Oort IM et al (2011) Prostate cancer: multiparametric MR imaging for detection, localization, and staging. Radiology 261(1):46–66
23. Malayeri AA, El Khouli RH, Zaheer A, Jacobs MA, Corona-Villalobos CP, Kamel IR, Macura KJ (2011) Principles and applications of diffusion-weighted imaging in cancer detection, staging, and treatment follow-up. Radiographics 31(6):1773–1791
24. Bihan DL (2013) Apparent diffusion coefficient and beyond: what diffusion MR imaging can tell us about tissue structure. Radiology 268(2):318–322
25. Zelhof B, Pickles M, Liney G, Gibbs P, Rodrigues G, Kraus S, Turnbull L (2009) Correlation of diffusion-weighted magnetic resonance data with cellularity in prostate cancer. BJU Int 103(7):883–888
26. Doo KW, Sung DJ, Park BJ, Kim MJ, Cho SB, Oh YW, Ko YH, Yang KS (2012) Detectability of low and intermediate or high risk prostate cancer with combined T2-weighted and diffusion-weighted MRI. Eur Radiol 22(8):1812–1819
27. van As NJ, de Souza NM, Riches SF, Morgan VA, Sohaib SA, Dearnaley DP, Parker CC (2009) A study of diffusion-weighted magnetic resonance imaging in men with untreated localised prostate cancer on active surveillance. Eur Urol 56(6):981–988
28. Tamada T, Sone T, Jo Y, Toshimitsu S, Yamashita T, Yamamoto A, Tanimoto D, Ito K (2008) Apparent diffusion coefficient values in peripheral and transition zones of the prostate: comparison between normal and malignant prostatic tissues and correlation with histologic grade. J Magn Reson Imaging 28(3):720–726
29. Turkbey B, Shah VP, Pang Y, Bernardo M, Xu S, Kruecker J, Locklin J, Baccala AA Jr, Rastinehad AR, Merino MJ et al (2011)Is apparent diffusion coefficient associated with clinical risk scores for prostate cancers that are visible on 3-T MR images? Radiology 258(2):488–495
30. Itou Y, Nakanishi K, Narumi Y, Nishizawa Y, Tsukuma H (2011) Clinical utility of apparent diffusion coefficient (ADC) values in patients with prostate cancer: can ADC values contribute to assess the aggressiveness of prostate cancer? J Magn Reson imaging 33(1):167–172
31. Hambrock T, Somford DM, Huisman HJ, van Oort IM, Witjes JA, de Kaa CAH, Scheenen T, Barentsz JO (2011) Relationship between apparent diffusion coefficients at 3.0-T MR imaging and Gleason grade in peripheral zone prostate cancer. Radiology 259(2):453–461
32. Wang X, Qian Y, Liu B, Cao L, Fan Y, Zhang JJ, Yu Y (2014) High-b value diffusion-weighted MRI for the detection of prostate cancer at 3 T. Clin Radiol 69(11):1165–1170
33. Rosenkrantz AB, Parikh N, Kierans AS, Kong MX, Babb JS, Taneja SS, Ream JM (2016) Prostate cancer detection using computed very high b value diffusion-weighted imaging: how high should we go? Acad Radiol 23(6):704–711
34. Shimofusa R, Fujimoto H, Akamata H, Motoori K, Yamamoto S, Ueda T, Ito H (2005) Diffusion-weighted imaging of prostate cancer. J Comput Assist Tomogr 29(2):149–153
35. Padhani AR (2011) Integrating multiparametric prostate MRI into clinical practice. Cancer Imaging 11(1A):S27
36. Barentsz JO, Jager G, Mugler JP, Oosterhof G, Peters H, Van Erning LT, Ruijs SH (1995) Staging urinary bladder cancer: value of T1-weighted three-dimensional magnetization prepared-rapid gradient-echo and two-dimensional spin-echo sequences. AJR Am J Roentgenol 164(1):109–115
37. Boetes C, Barentsz JO, Mus RD, Van Der Sluis RF, van Erning LJ, Hendriks JH, Holland R, Ruys SH (1994) MR characterization of suspicious breast lesions with a gadolinium-enhanced TurboFLASH subtraction technique. Radiology 193(3):777–781
38. Hanahan D, Weinberg Ra (2011) Hallmarks of cancer: the next generation. Cell 144(5):646–674
39. Weidner N, Carroll PR, Flax J, Blumenfeld W, Folkman J (1993) Tumor angiogenesis correlates with metastasis in invasive prostate carcinoma. Am J Pathol 143(2):401
40. Brawer MK, Deering RE, Brown M, Preston SD, Bigler SA (1994) Predictors of pathologic stage in prostatic carcinoma. The role of neovascularity. Cancer 73(3):678–687
41. Siegal JA, Yu E, Brawer MK (1995) Topography of neovascularity in human prostate carcinoma. Cancer 75(10):2545–2551
42. Coakley FV, Hricak H (2000) Radiologic anatomy of the prostate gland: a clinical approach. Radiol Clin North Am 38(1):15–30
43. Viliers A, Steg A, Boccon-Gibod L (1991) Anatomy of the prostate: review of the different models. Eur Urol 20:261–268
44. Verma S, Turkbey B, Muradyan N, Rajesh A, Cornud F, Haider Ma, Choyke PL, Harisinghani M (2012) Overview of dynamic contrast-enhanced MRI in prostate cancer diagnosis and management. Am J Roentgenol 198(6):1277–1288
45. Gribbestad IS, Gjesdal KI, Nilsen G, Lundgren S, Hjelstuen MHB, Jackson A (2005) An introduction to dynamic contrast-enhanced MRI in oncology. In: Jackson A, Buckley DL, Parker

GJM (eds) dynamic contrast-enhanced magnetic resonance imaging in oncology. Springer, Berlin, pp 1–22
46. Huisman HJ, Engelbrecht MR, Barentsz JO (2001) Accurate estimation of pharmacokinetic contrast-enhanced dynamic MRI parameters of the prostate. J Magn Reson Imaging 13(4):607–614
47. Alonzi R, Padhani AR, Allen C (2007) Dynamic contrast enhanced MRI in prostate cancer. Eur J Radiol 63(3):335–350
48. Hansford BG, Peng Y, Jiang Y, Vannier MW, Antic T, Thomas S, McCann S, Oto A (2015) Dynamic contrast-enhanced MR imaging curve-type analysis: is it helpful in the differentiation of prostate cancer from healthy peripheral zone? Radiology 275(2):448–457
49. Engelbrecht MR, Huisman HJ, Laheij RJF, Jager GJ, van Leenders GJLH, Hulsbergen-Van CA, De Kaa JJ, de la Rosette JG, Blickman, Barentsz JO (2003) Discrimination of prostate cancer from normal peripheral zone and central gland tissue by using dynamic contrast-enhanced MR imaging. Radiology 229(1):248–254
50. Jackson ASN, Reinsberg SA, Sohaib SA, Charles-Edwards EM, Jhavar S, Christmas TJ, Thompson AC, Bailey MJ, Corbishley CM, Fisher C et al. (2009) Dynamic contrast-enhanced MRI for prostate cancer localization. Br J Radiol 82(974):148–156
51. Kiessling F, Lichy M, Grobholz R, Heilmann M, Farhan N, Michel MS, Trojan L, Ederle J, Abel U, Kauczor H-U et al. (2004) Simple models improve the discrimination of prostate cancers from the peripheral gland by T1-weighted dynamic MRI. Eur Radiol 14(10):1793–1801
52. Tofts PS, Wicks DA, Barker GJ (1991) The MRI measurement of NMR and physiological parameters in tissue to study disease process. Prog Clin Biol Res 363:313–325
53. Brix G, Semmler W, Port R, Schad LR, Layer G, Lorenz WJ (1991) Pharmacokinetic parameters in CNS Gd-DTPA enhanced MR imaging. J Comput Assist Tomogr 15(4):621–628
54. Larsson HBW, Stubgaard M, Frederiksen JL, Jensen M, Henriksen O, Paulson OB (1990) Quantitation of blood–brain barrier defect by magnetic resonance imaging and gadolinium-DTPA in patients with multiple sclerosis and brain tumors. Magn Reson Med 16(1):117–131
55. Puech P, Sufana-Iancu A, Renard B, Lemaitre L (2013) Prostate MRI: can we do without DCE sequences in 2013? Diagn Interv Imaging 94(12):1299–1311
56. Awwad HM, Geisel J, Obeid R (2012) The role of choline in prostate cancer. Clin Biochem 45(18):1548–1553
57. Costello LC, Franklin RB (2006) The clinical relevance of the metabolism of prostate cancer; zinc and tumor suppression: connecting the dots. Mol Cancer 5(1):17
58. Giskeødegård GF, Bertilsson H, Selnæs KM, Wright AJ, Bathen TF, Viset T, Halgunset J, Angelsen A, Gribbestad IS, Tessem M-B (2013) Spermine and citrate as metabolic biomarkers for assessing prostate cancer aggressiveness. PLoS One 8(4):e62375
59. Robert D, Andra M, Bruce B, Alexander L, Kenneth P (1998) Functional magnetic resonance imaging: the basics of blood-oxygen-level dependent (BOLD) imaging. Can Assoc Radiol J 5:1–12
60. Prasad PV, Edelman RR, Epstein FH (1996) Noninvasive evaluation of intrarenal oxygenation with BOLD MRI. Circulation 94(12):3271–3275
61. Hoskin PJ, Carnell DM, Taylor NJ, Smith RE, Stirling JJ, Daley FM, Saunders MI, Bentzen SM, Collins DJ, D'Arcy JA, Padhani AP (2007) Hypoxia in prostate cancer: correlation of BOLD-MRI With pimonidazole immunohistochemistry—initial observations. Int J Radiat Oncol 68(4):1065–1071
62. Di N, Mao N, Cheng W, Pang H, Ren Y, Wang N, Liu X, Wang B (2016) Blood oxygenation level-dependent magnetic resonance imaging during carbogen breathing: differentiation between prostate cancer and benign prostate hyperplasia and correlation with vessel maturity. Onco Targets Ther 9:4143
63. Perera M, Krishnananthan N, Lindner U, Lawrentschuk N (2016) An update on focal therapy for prostate cancer. Nat Rev Urol 13(11):641–653
64. Babaian RJ, Toi A, Kamoi K, Troncoso P, Sweet J, Evans R, Johnston D, Chen M (2000) A comparative analysis of sextant and an extended 11-core multisite directed biopsy strategy. J Urol 163(1):152–157
65. Presti JC, O'dowd GJ, Miller MC, Mattu R, Veltri RW (2003) Extended peripheral zone biopsy schemes increase cancer detection rates and minimize variance in prostate specific antigen and age related cancer rates: results of a community multi-practice study. J Urol 169(1):125–129
66. Eskew LA, Bare RL, McCullough DL (1997) Systematic 5 region prostate biopsy is superior to sextant method for diagnosing carcinoma of the prostate. J Urol 157(1):199–203
67. Zamecnik P, Schouten MG, Krafft AJ, Maier F, Schlemmer H-P, Barentsz JO, Bock M, Fütterer JJ (2014) Automated real-time needle-guide tracking for fast 3-T MR-guided transrectal prostate biopsy: a feasibility study. Radiology 273(3):879–886
68. Vourganti S, Rastinehad A, Yerram NK, Nix J, Volkin D, Hoang A, Turkbey B, Gupta GN, Kruecker J, Linehan WM, Choyke PL, Wood BJ, Pinto PA (2012) Multiparametric magnetic resonance imaging and ultrasound fusion biopsy detect prostate cancer in patients with prior negative transrectal ultrasound biopsies. J Urol 188(6):2152–2157
69. Delongchamps NB, Rouanne M, Flam T, Beuvon F, Liberatore M, Zerbib M, Cornud F (2011) Multiparametric magnetic resonance imaging for the detection and localization of prostate cancer: combination of T2-weighted, dynamic contrast-enhanced and diffusion-weighted imaging. BJU Int 107(9):1411–1418
70. Lemaitre L, Puech P, Poncelet E, Bouyé S, Leroy X, Biserte J, Villers A (2009) Dynamic contrast-enhanced MRI of anterior prostate cancer: morphometric assessment and correlation with radical prostatectomy findings. Eur Radiol 19(2):470–480
71. Puech P, Potiron E, Lemaitre L, Leroy X, Haber G-P, Crouzet S, Kamoi K, Villers A (2009) Dynamic contrast-enhanced–magnetic resonance imaging evaluation of intraprostatic prostate cancer: correlation with radical prostatectomy specimens. Urology 74(5):1094–1099
72. Moore CM, Robertson NL, Arsanious N, Middleton T, Villers A, Klotz L, Taneja SS, Emberton M (2017) image-guided prostate biopsy using magnetic resonance imaging–derived targets: a systematic review. Eur. Urol 63(1):125–140
73. Siddiqui M, Rais-Bahrami S, Turkbey B et al (2015) Comparison of mr/ultrasound fusion–guided biopsy with ultrasound-guided biopsy for the diagnosis of prostate cancer. JAMA 313(4):390–397
74. Watanabe Y, Terai A, Araki T, Nagayama M, Okumura A, Amoh Y, Ishimori T, Ishibashi M, Nakashita S, Dodo Y (2012) Detection and localization of prostate cancer with the targeted biopsy strategy based on ADC Map: a prospective large-scale cohort study. J Magn Reson Imaging 35(6):1414–1421
75. Turkbey B, Mani H, Aras O, Rastinehad AR, Shah V, Bernardo M, Pohida T, Daar D, Benjamin C, McKinney YL et al. (2012) Correlation of magnetic resonance imaging tumor volume with histopathology. J Urol 188(4):1157–1163
76. Oto A, Yang C, Kayhan A, Tretiakova M, Antic T, Schmid-Tannwald C, Eggener S, Karczmar GS, Stadler WM (2011) Diffusion-weighted and dynamic contrast-enhanced MRI of prostate cancer: correlation of quantitative MR parameters with Gleason score and tumor angiogenesis. Am J Roentgenol 197(6):1382–1390
77. Hambrock T, Hoeks C, de Kaa CH, Scheenen T, Fütterer J, Bouwense S, van Oort I, Schröder F, Huisman H, Barentsz J (2012)

Prospective assessment of prostate cancer aggressiveness using 3-t diffusion-weighted magnetic resonance imaging–guided biopsies versus a systematic 10-core transrectal ultrasound prostate biopsy cohort. Eur Urol 61(1):177–184
78. Kobus T, Vos PC, Hambrock T, De Rooij M, de Kaa CAH, Barentsz JO, Heerschap A, Scheenen TWJ (2012) Prostate cancer aggressiveness: in vivo assessment of mr spectroscopy and diffusion-weighted imaging at 3 T. Radiology 265(2):457–467
79. Vargas HA, Akin O, Franiel T, Mazaheri Y, Zheng J, Moskowitz C, Udo K, Eastham J, Hricak H (2011) Diffusion-weighted endorectal MR imaging at 3 T for prostate cancer: tumor detection and assessment of aggressiveness. Radiology 259(3):775–784
80. Verma S, Rajesh A, Morales H, Lemen L, Bills G, Delworth M, Gaitonde K, Ying J, Samartunga R, Lamba M (Feb. 2011) Assessment of aggressiveness of prostate cancer: correlation of apparent diffusion coefficient with histologic grade after radical prostatectomy. Am J Roentgenol 196(2):374–381
81. Woodfield Ca, Tung Ga, Grand DJ, Pezzullo Ja, Machan JT, Renzulli JF (2010) Diffusion-weighted MRI of peripheral zone prostate cancer: comparison of tumor apparent diffusion coefficient with Gleason score and percentage of tumor on core biopsy. Int Braz J Urol 36(4):504
82. Vos EK, Litjens GJS, Kobus T, Hambrock T, De Kaa CAH, Barentsz JO, Huisman HJ, Scheenen TWJ (2013) Assessment of prostate cancer aggressiveness using dynamic contrast-enhanced magnetic resonance imaging at 3 T. Eur Urol 64(3):448–455
83. Peng Y, Jiang Y, Yang C, Brown JB, Antic T, Sethi I, Schmid-Tannwald C, Giger ML, Eggener SE, Oto A (2013) Quantitative analysis of multiparametric prostate MR images: differentiation between prostate cancer and normal tissue and correlation with Gleason score—a computer-aided diagnosis development study. Radiology 267(3):787–796
84. Nagarajan R, Margolis D, Raman S, Sarma MK, Sheng K, King CR, Verma G, Sayre J, Reiter RE, Thomas MA (2012) MR spectroscopic imaging and diffusion-weighted imaging of prostate cancer with Gleason scores. J Magn Reson Imaging 36(3):697–703
85. Augustin H, Eggert T, Wenske S, Karakiewicz PI, Palisaar J, Daghofer F, Huland H, Graefen M (2004) Comparison of accuracy between the partin tables of 1997 and 2001 to predict final pathological stage in clinically localized prostate cancer. J Urol 171(1):177–181
86. Augustin H, Fritz GA, Ehammer T, Auprich M, Pummer K (2009) Accuracy of 3-Tesla magnetic resonance imaging for the staging of prostate cancer in comparison to the Partin tables. Acta radiol 50(5):562–569
87. Dickinson L, Ahmed HU, Allen C, Barentsz JO, Carey B, Futterer JJ, Heijmink SW, Hoskin PJ, Kirkham A, Padhani AR, Persad R, Puech P, Punwani S, Sohaib AS, Tombal B, Villers A, van der Meulen J, Emberton M (2011) Magnetic resonance imaging for the detection, localisation, and characterisation of prostate cancer: recommendations from a European consensus meeting Eur Urol 59:477–494
88. Renard-Penna R, Rouprêt M, Comperat E, Ayed A, Coudert M, Mozer P, Xylinas E, Bitker M-O, Grenier P (2013) Accuracy of high resolution (1.5 T) pelvic phased array magnetic resonance imaging (MRI) in staging prostate cancer in candidates for radical prostatectomy: results from a prospective study. Urol Oncol 31(4):448–454
89. Fütterer JJ, Heijmink SW, Scheenen TWJ, Jager GJ, de Kaa CA, Witjes JA, Barentsz JO (2006) Prostate cancer: local staging at 3-T endorectal MR imaging—early experience Radiology 238(1):184–191
90. McClure TD, Margolis DJA, Reiter RE, Sayre JW, Thomas MA, Nagarajan R, Gulati M, Raman SS (2012) Use of MR imaging to determine preservation of the neurovascular bundles at robotic-assisted laparoscopic prostatectomy. Radiology 262(3):874–883
91. Rosenkrantz AB, Scionti SM, Mendrinos S, Taneja SS (2011) Role of MRI in minimally invasive focal ablative therapy for prostate cancer. Am J Roentgenol 197(1):W90–W96
92. Le JD, Tan N, Shkolyar E, Lu DY, Kwan L, Marks LS, Huang J, Margolis DJA, Raman SS, Reiter RE (2015) Multifocality and prostate cancer detection by multiparametric magnetic resonance imaging: correlation with whole-mount histopathology. Eur Urol 67(3):569–576
93. Baco E, Ukimura O, Rud E, Vlatkovic L, Svindland A, Aron M, Palmer S, Matsugasumi T, Marien A, Bernhard J-C et al.(2015) Magnetic resonance imaging–transectal ultrasound image-fusion biopsies accurately characterize the index tumor: correlation with step-sectioned radical prostatectomy specimens in 135 patients. Eur Urol 67(4):787–794
94. Rud E, Klotz D, Rennesund K, Baco E, Berge V, Lien D, Svindland A, Lundeby E, Berg RE, Eri LM, Eggesbø HB (2014) Detection of the index tumour and tumour volume in prostate cancer using T2-weighted and diffusion-weighted magnetic resonance imaging (MRI) alone. BJU Int 114(6b):E32–E42
95. Tan N, Margolis DJ, Lu DY, King KG, Huang J, Reiter RE, Raman SS (2015) Characteristics of detected and missed prostate cancer foci on 3-T multiparametric MRI using an endorectal coil correlated with whole-mount thin-section histopathology. Am J Roentgenol 205(1):W87–W92
96. Lambin P, Rios-Velazquez E, Leijenaar R, Carvalho S, van Stiphout RGPM, Granton P, Zegers CML, Gillies R, Boellard R, Dekker A, Aerts HJ (2012) Radiomics: extracting more information from medical images using advanced feature analysis. Eur J Cancer 48(4):441–446
97. Aerts HJWL, Velazquez ER, Leijenaar RTH, Parmar C, Grossmann P, Cavalho S, Bussink J, Monshouwer R, Haibe-Kains B, Rietveld D, Hoebers F, Rietbergen MM, Leemans CR, Dekker A, Quackenbush J, Gillies RJ, Lambin P (2014) Decoding tumour phenotype by noninvasive imaging using a quantitative radiomics approach. Nat. Commun. 5:4006
98. Gillies RJ, Kinahan PE, Hricak H (2016) Radiomics: images are more than pictures, they are data. Radiology 278(2):563–577
99. O'connor JPB, Aboagye EO, Adams JE, Aerts HJWL, Barrington SF, Beer AJ, Boellaard R, Bohndiek SE, Brady M, Brown G et al. (2016) Imaging biomarker roadmap for cancer studies. Nat Rev Clin Oncol 14(3):169–186
100. Parmar C, Rios Velazquez E, Leijenaar R, Jermoumi M, Carvalho S, Mak RH, Mitra S, Shankar BU, Kikinis R, Haibe-Kains B, Lambin P, Aerts HJWL (2014) Robust radiomics feature quantification using semiautomatic volumetric segmentation. PLoS One 9(7):1–8
101. Asselin M, Connor JPBO, Boellaard R, Thacker NA, Jackson A (2012) Quantifying heterogeneity in human tumours using MRI and PET. Eur J Cancer 48(4):447–455
102. Yip SSF, Aerts HJWL (2016) Applications and limitations of radiomics. Phys Med Biol 61(13):R150
103. Dekker A, Vinod S, Holloway L, Oberije C, George A, Goozee G, Delaney GP, Lambin P, Thwaites D (2014) Rapid learning in practice: a lung cancer survival decision support system in routine patient care data. Radiother Oncol 113(1):47–53
104. Giger ML, Chan H-P, Boone J (2008) Anniversary paper: history and status of CAD and quantitative image analysis: the role of medical physics and AAPM. Med Phys 35(12):5799–5820
105. Artan Y, Langer DL, Haider MA, van der Kwast TH, Evans AJ, Wernick MN, Yetik IS (2009) Prostate cancer segmentation with multispectral MRI using cost-sensitive conditional random fields., In Biomedical Imaging: from Nano to Macro, ISBI'09. IEEE International Symposium on, 2009, pp. 278–281

106. Artan Y, Haider Ma, Langer DL, Van Der Kwast TH, Evans AJ, Yang Y, Wernick MN, Trachtenberg J, Yetik IS (2010) Prostate cancer localization with multispectral MRI using cost-sensitive support vector machines and conditional random fields. IEEE Trans Image Process 19(9):2444–2455
107. Matulewicz L, Jansen JF, Bokacheva L, Vargas H, Akin O, Fine SW, a Shukla-Dave J a Eastham H, Hricak J, Koutcher, Zakian KL (2013) Anatomic segmentation improves prostate cancer detection with artificial neural networks analysis of H magnetic resonance spectroscopic imaging. J Magn Reson Imaging 1421:1414–1421
108. Niaf E, Rouvière O, Lartizien C (2011) Computer-aided diagnosis for prostate cancer detection in the peripheral zone via multisequence MRI. In: Proc. SPIE 7963, Medical Imaging 2011: Computer-Aided Diagnosis, 79633P. https://doi.org/10.1117/12.877231
109. Niaf E, Rouvière O, Mège-Lechevallier F, Bratan F, Lartizien C (2012) Computer-aided diagnosis of prostate cancer in the peripheral zone using multiparametric MRI. Phys Med Biol 57(12):3833
110. Ozer S, Haider MA, Langer DL, van der Kwast TH, Evans AJ, Wernick MN, Trachtenberg J, Yetik IS (2009) Prostate cancer localization with multispectral MRI based on Relevance Vector Machines. In: 2009 IEEE International Symposium on Biomedical Imaging: from Nano to Macro, Boston, MA, pp. 73–76. https://ieeexplore.ieee.org/abstract/document/5192986
111. Ozer S, Langer DL, Liu X, Haider MA, van der Kwast TH, Evans AJ, Yang Y, Wernick MN, Yetik IS (2010) Supervised and unsupervised methods for prostate cancer segmentation with multispectral MRI. Med Phys 37(4):1873–1883
112. Puech P, Betrouni N, Makni N, Dewalle A-S, Villers A, Lemaitre L (2009) Computer-assisted diagnosis of prostate cancer using DCE-MRI data: design, implementation and preliminary results. Int J Comput Assist Radiol Surg 4(1):1–10
113. Vos PC, Hambrock T, Barentsz JO, Huisman HJ (2008) Combining T2-weighted with dynamic MR images for computerized classification of prostate lesions. In: Proc. SPIE 6915, Medical Imaging 2008: Computer-Aided Diagnosis, 69150W. https://doi.org/10.1117/12.771970
114. Vos PC, Hambrock T, Hulsbergen C - van de Kaa JJ, Fütterer JO, Barentsz, Huisman HJ (2008) Computerized analysis of prostate lesions in the peripheral zone using dynamic contrast enhanced MRI. Med Phys 35(3):888
115. Martin S, Troccaz J, Daanen V (2010) Automated segmentation of the prostate in 3D MR images using a probabilistic atlas and a spatially constrained deformable model. Med Phys 37(4):1579–1590
116. Yin Y, Fotin SV, Periaswamy S, Kunz J, Haldankar H, Muradyan N, Cornud F, Turkbey B, Choyke PL (2012) Fully automated prostate segmentation in 3D MR based on normalized gradient fields cross-correlation initialization and LOGISMOS refinement. In: Medical Imaging 2012:8314. https://doi.org/10.1117/12.911758
117. Dowling JA, Fripp J, Chandra S, Pluim JPW, Lambert J, Parker J, Denham J, Greer PB, Salvado O (2011) Fast automatic multiatlas segmentation of the prostate from 3D MR images. In: Madabhushi A, Dowling J, Huisman H, Barratt D (eds) Prostate cancer imaging. Image analysis and image-guided interventions. Prostate cancer imaging 2011. Lecture notes in computer science, vol 6963. Springer, Berlin, pp. 10–21. https://doi.org/10.1007/978-3-642-23944-1_2
118. Ou Y, Doshi J, Erus G, Davatzikos C (2012) Multi-atlas segmentation of the prostate: a zooming process with robust registration and atlas selection.MICCAI Gd Chall Prostate MR Image Segm 7
119. Litjens G, Karssemeijer N, Huisman H (2012) A multi-atlas approach for prostate segmentation in MR images MICCAI Gd Chall Prostate MR Image Segm 2018
120. Cootes TF, Edwards GJ, Taylor CJ (2001) Active appearance models. IEEE Trans Pattern Anal Mach Intell 23(6):681–685
121. Vincent G, Guillard G, Bowes M (2012) Fully automatic segmentation of the prostate using active appearance models MICCAI Gd Chall Prostate MR Image Segm 2012:7
122. Viswanath S, Bloch BN, Rosen M, Chappelow J, Toth R, Rofsky N, Lenkinski R, Genega E, Kalyanpur A, Madabhushi A (2009) Integrating structural and functional imaging for computer assisted detection of prostate cancer on multi-protocol in vivo 3 T MRI. Proc SPIE Int Soc Opt Eng 7260:72603I
123. Viswanath S, Bloch BN, Genega E, Rofsky N, Lenkinski R, Chappelow J, Toth R, Madabhushi A (2008) A comprehensive segmentation, registration, and cancer detection scheme on 3 T in vivo prostate DCE-MRI. Lect Notes Comput Sci (Incl Subser Lect Notes Artif Intell Lect Notes Bioinf) 5241(Part1):662–669
124. Xie S, Tu Z (2015) Holistically-nested edge detection. IEEE Int Conf Comput Vis (ICCV) 2015:1395–1403
125. Zhu Q, Du B, Turkbey B, Choyke PL, Yan P (2017) Deeply-Supervised CNN for Prostate Segmentation. arXiv Prepr. arXiv1703.07523
126. Ampeliotis D, Antonakoudi A, Berberidis K, Psarakis EZ (2007) Computer aided detection of prostate cancer using fused information from dynamic contrast enhanced and morphological magnetic resonance images. In: 2007 IEEE International Conference on Signal Processing and Communications, Dubai. pp. 888–891. https://ieeexplore.ieee.org/document/4728462
127. Ampeliotis D, Antonakoudi A, Berberidis K, Psarakis EZ, Kounoudes A (2008) A computer-aided system for the detection of prostate cancer based on magnetic resonance image analysis. In: 2008 3rd International Symposium on Communications, Control and Signal Processing, St Julians. pp. 1372–1377. https://ieeexplore.ieee.org/document/4537440
128. Viswanath S, Bloch BN, Chappelow J, Patel P, Rofsky N, Lenkinski R, Genega E, Madabhushi A (2011) Enhanced multi-protocol analysis via intelligent supervised embedding (EMPrAvISE): detecting prostate cancer on multi-parametric MRI. Proc SPIE Int Soc Opt Eng 7963:79630U
129. Litjens G, Toth R, Van de Ven W, Hoeks C, Kerkstra S, Van Ginneken B (2014) Evaluation of prostate segmentation algorithms for MRI: the PROMISE12 challenge. Med Image Anal 18(2):359–373
130. Giannini V, Vignati A, Mazzetti S, De Luca M, Bracco C, Stasi M, Russo F, Armando E, Regge D (2013) A prostate CAD system based on multiparametric analysis of DCE T1-w, and DW automatically registered images. Proc SPIE 8670:86703E
131. Vos PC, Hambrock T, Barenstz JO, Huisman HJ (2010) Computer-assisted analysis of peripheral zone prostate lesions using T2-weighted and dynamic contrast enhanced T1-weighted MRI. Phys Med Biol 55(6):1719–1734
132. Peng Y, Jiang Y, Antic T, Giger ML, Eggener S, Oto A (2013) A study of T2-weighted MR image texture features and diffusion-weighted MR image features for computer-aided diagnosis of prostate cancer. Proc SPIE 8670:86701H
133. Peng Y, Jiang Y, Antic T, Giger ML, Eggener SE, Oto A (2014) Validation of quantitative analysis of multiparametric prostate mr images for prostate cancer detection and aggressiveness assessment: a cross-imager study. Radiology 271(2):461–471
134. Commandeur F, Acosta O, Simon A, Mathieu R, Fautrel A, Gnep K, Haigron P, de Crevoisier R (2015) Prostate whole-mount histology reconstruction and registration to MRI for correlating in-vivo observations with biological findings. In: engineering in medicine and biology society (EMBC), 37th annual international conference of the IEEE, pp. 2399–2402

135. Xiao G, Bloch BN, Chappelow J, Genega EM, Rofsky NM, Lenkinski RE, Tomaszewski J, Feldman MD, Rosen M, Madabhushi A (2011) Determining histology-MRI slice correspondences for defining MRI-based disease signatures of prostate cancer. Comput Med Imaging Graph 35(7):568–578
136. Chappelow J, Bloch BN, Rofsky N, Genega E, Lenkinski R, DeWolf W, Madabhushi A (2011) Elastic registration of multimodal prostate MRI and histology via multiattribute combined mutual information. Med Phys 38(4):2005–2018
137. Chappelow J, Madabhushi A, Rosen M, Tomaszeweski J, Feldman M (2007) Multimodal image registration of ex vivo 4 T MRI with whole mount histology for prostate cancer detection. Med Imaging 6512:65121S
138. Patel P, Chappelow J, Tomaszewski J, Feldman MD, Rosen M, Shih N, Madabhushi A (2011) Spatially weighted mutual information (SWMI) for registration of digitally reconstructed ex vivo whole mount histology and in vivo prostate MRI. In: engineering in medicine and biology society, EMBC, annual international conference of the IEEE, pp. 6269–6272
139. Park H, Piert MR, Khan A, Shah R, Hussain H, Siddiqui J, Chenevert TL, Meyer CR (2008) Registration methodology for histological sections and in vivo imaging of human prostate. Acad Radiol 15(8):1027–1039
140. Gibson E, Crukley C, Gaed M, Gómez JA, Moussa M, Chin JL, Bauman GS, Fenster A, Ward AD (2012) Registration of prostate histology images to ex vivo MR images via strand-shaped fiducials. J Magn Reson Imaging 36(6):1402–1412
141. Turkbey B, Mani H, Shah V, Rastinehad AR, Bernardo M, Pohida T, Pang Y, Daar D, Benjamin C, McKinney YL, Trivedi H, Chua C, Bratslavsky G, Shih JH, Linehan WM, Merino MJ, Choyke PL, Pinto PA (2011) Multiparametric 3T prostate magnetic resonance imaging to detect cancer: histopathological correlation using prostatectomy specimens processed in customized magnetic resonance imaging based molds. J Urol 186(5):1818–1824
142. Bourne RM, Bailey C, Johnston EW, Pye H, Heavey S, Whitaker H, Siow B, Freeman A, Shaw GL, Sridhar A (2017) et al Apparatus for histological validation of in vivo and ex vivo magnetic resonance imaging of the human prostate. Front. Oncol 7:47
143. Shah V, Pohida T, Turkbey B, Mani H, Merino M, Pinto PA, Choyke P, Bernardo M (2009) A method for correlating in vivo prostate magnetic resonance imaging and histopathology using individualized magnetic resonance-based molds. Rev Sci Instrum 80(10):104301
144. Priester A, Natarajan S, Le JD, Garritano J, Radosavcev B, Grundfest W, Margolis DJA, Marks LS, Huang J (2014) A system for evaluating magnetic resonance imaging of prostate cancer using patient-specific 3D printed molds. Am J Clin Exp Urol 2(2):127
145. Orczyk C, Taneja SS, Rusinek H, Rosenkrantz AB (2014) Assessment of change in prostate volume and shape following surgical resection through co-registration of in-vivo MRI and fresh specimen ex-vivo MRI. Clin Radiol 69(10):e398–e403
146. Reynolds HM, Williams S, Zhang A, Chakravorty R, Rawlinson D, Ong CS, Esteva M, Mitchell C, Parameswaran B, Finnegan M, Liney G, Haworth A (2015) Development of a registration framework to validate MRI with histology for prostate focal therapy. Med. Phys 42(12):7078–7089
147. Niaf E, Rouvière O, Mège-Lechevallier F, Bratan F, Lartizien C (2012) Computer-aided diagnosis of prostate cancer in the peripheral zone using multiparametric MRI. Phys Med Biol 57(12):3833–3851
148. Tiwari P, Rosen M, Reed G, Kurhanewicz J, Madabhushi A (2009) Spectral embedding based probabilistic boosting tree (ScEPTre): classifying high dimensional heterogeneous biomedical data. Lect Notes Comput Sci 5762 LNCS(PART 2):844–851
149. Tiwari P, Kurhanewicz J, Rosen M, Madabhushi A (2010) Semi supervised multi-kernel (SeSMiK) graph embedding: identifying aggressive prostate cancer via magnetic resonance imaging and spectroscopy. Int Conf Med Image Comput Comput Assist Interv 13(3):666–673
150. Tiwari P, Kurhanewicz J, Madabhushi A (2013) Multi-kernel graph embedding for detection, Gleason grading of prostate cancer via MRI/MRS. Med Image Anal 17(2):219–235
151. Viswanath S, Tiwari P, Rosen M, Madabhushi A (2008) A meta-classifier for detecting prostate cancer by quantitative integration of in vivo magnetic resonance spectroscopy and magnetic resonance imaging. SPIE Med Imaging 6915:69153D
152. Vos PC, Barentsz JO, Karssemeijer N, Huisman HJ (2012) Automatic computer-aided detection of prostate cancer based on multiparametric magnetic resonance image analysis. Phys Med Biol 57(6):1527–1542
153. Li Q, Sone S, Doi K (2003) Selective enhancement filters for nodules, vessels, and airway walls in two- and three-dimensional CT scans. Med Phys 30(8):2040–2051
154. Litjens GJS, Barentsz JO, Karssemeijer N, Huisman HJ (2012) Automated computer-aided detection of prostate cancer in MR images: from a whole-organ to a zone-based approach. Prog Biomed Opt Imaging Proc SPIE 8315:83150G
155. Litjens GJS, Vos PC, Barentsz JO, Karssemeijer N, Huisman HJ (2011) Automatic computer aided detection of abnormalities in multi-parametric prostate MRI. Proc. SPIE 7963:79630T–79630T–7
156. Litjens G, Debats O, Barentsz J, Karssemeijer N, Huisman H (2014) Computer-aided detection of prostate cancer in MRI. IEEE Trans Med Imaging 33(5):1083–1092
157. Haralick RM, Shanmugam K, Dinstein I (1973) Textural Features for Image Classification. IEEE Trans Syst Man Cybern 3(6):610–621
158. Haralick RM (1979) Statistical and structural approaches to texture. Proc IEEE 67(5):786–804
159. Galloway MM (1975) Texture analysis using gray level run lengths. Comput Graph Image Process 4(2):172–179
160. Thibault G, Fertil B, Navarro C, Pereira S, Cau P, Levy N, Sequeira J, Mari J-L (2013) Shape and texture indexes application to cell nuclei classification. Int J Pattern Recognit Artif Intell 27(1):1357002
161. Kuess P, Andrzejewski P, Nilsson D, Georg P, Knoth J, Susani M, Trygg J, Helbich TH, Polanec SH, Georg D et al (2017) Association between pathology and texture features of multi parametric MRI of the prostate. Phys Med Biol 62(19):7833
162. Chung AG, Khalvati F, Shafiee MJ, Haider MA, Wong A (2015) Prostate cancer detection via a quantitative radiomics-driven conditional random field framework. IEEE Access 3:2531–2541
163. Chung AG, Shafiee MJ, Kumar D, Khalvati F, Haider MA, Wong A (2015) Discovery radiomics for multi-parametric mri prostate cancer detection. arXiv Prepr. arXiv:1509.00111,
164. Ginsburg SB, Algohary A, Pahwa S, Gulani V, Ponsky L, Aronen HJ, Boström PJ, Böhm M, Haynes A-M, Brenner P et al (2017) Radiomic features for prostate cancer detection on MRI differ between the transition and peripheral zones: preliminary findings from a multi-institutional study. J Magn Reson Imaging 46(1):184–193
165. Iyama Y, Nakaura T, Katahira K, Iyama A, Nagayama Y, Oda S, Utsunomiya D, Yamashita Y (2017) Development and validation of a logistic regression model to distinguish transition zone cancers from benign prostatic hyperplasia on multi-parametric prostate MRI. Eur Radiol 27:1–9
166. Viswanath SE, Bloch NB, Chappelow JC, Toth R, Rofsky NM, Genega EM, Lenkinski RE, Madabhushi A (2012) Central gland and peripheral zone prostate tumors have significantly

different quantitative imaging signatures on 3 T endorectal, in vivo T2-weighted MR imagery. J Magn Reson Imaging 36(1):213–224
167. Taira AV, Merrick GS, Galbreath RW, Andreini H, Taubenslag W, Curtis R, Butler WM, Adamovich E, Wallner KE (2010) Performance of transperineal template-guided mapping biopsy in detecting prostate cancer in the initial and repeat biopsy setting. Prostate Cancer Prostatic Dis 13(1):71–77
168. Delongchamps NB, Peyromaure M, Schull A, Beuvon F, Bouazza N, Flam T, Zerbib M, Muradyan N, Legman P, Cornud F (2013) Prebiopsy magnetic resonance imaging and prostate cancer detection: comparison of random and targeted biopsies. J Urol 189(2):493–499
169. Ghose S, Oliver A, Mart'\i R, Lladó X, Vilanova JC, Freixenet J, Mitra J, Sidibé D, Meriaudeau F (2012) A survey of prostate segmentation methodologies in ultrasound, magnetic resonance and computed tomography images. Comput Methods Programs Biomed 108(1):262–287
170. Tiwari P, Rosen M, Madabhushi A (2009) A hierarchical spectral clustering and nonlinear dimensionality reduction scheme for detection of prostate cancer from magnetic resonance spectroscopy (MRS). Med Phys 36(9):3927–3939
171. Tiwari P, Rosen M, Madabhushi A (2008) Consensus-locally linear embedding (C-LLE): application to prostate cancer detection on magnetic resonance spectroscopy. Med image Comput Comput Interv MICCAI 11(Pt 2):330–338
172. Tiwari P, Madabhushi A, Rosen M (2007) A Hierarchical unsupervised spectral clustering scheme for detection of prostate cancer from magnetic resonance spectroscopy (MRS). Society: 278–286
173. Niu X, Li J, Das SK, Xiong Y, Yang C, Peng T (2017) Developing a nomogram based on multiparametric magnetic resonance imaging for forecasting high-grade prostate cancer to reduce unnecessary biopsies within the prostate-specific antigen gray-zone. BMC Med Imaging 17(1):11–19
174. Langer DL, van der Kwast TH, Evans AJ, Trachtenberg J, Wilson BC, Haider MA (2009) Prostate cancer detection with multi-parametric MRI: logistic regression analysis of quantitative T2, diffusion-weighted imaging, and dynamic contrast-enhanced MRI. J Magn Reson imaging 30(2):327–334
175. Dikaios N, Alkalbani J, Sidhu HS, Fujiwara T, Abd-Alazeez M, Kirkham A, Allen C, Ahmed H, Emberton M, Freeman A et al (2015) Logistic regression model for diagnosis of transition zone prostate cancer on multi-parametric MRI. Eur Radiol 25(2):523–532
176. Dikaios N, Alkalbani J, Abd-Alazeez M, Sidhu HS, Kirkham A, Ahmed HU, Emberton M, Freeman A, Halligan S, Taylor S, Atkinson D, Punwani S (2015) Zone-specific logistic regression models improve classification of prostate cancer on multi-parametric MRI. Eur Radiol 25(9):2727–2737
177. Shah V, Turkbey B, Mani H, Pang Y, Pohida T, Merino MJ, Pinto PA, Choyke PL, Bernardo M (2012) Decision support system for localizing prostate cancer based on multiparametric magnetic resonance imaging. Med Phys 39(7):4093
178. Lay N, Tsehay Y, Greer MD, Turkbey B, Kwak JT, Choyke PL, Pinto P, Wood BJ, Summers RM (2017) Detection of prostate cancer in multiparametric MRI using random forest with instance weighting. J Med Imaging 4(2):24506
179. Qian C, Wang L, Yousuf A, Oto A, Shen D (2014) In vivo MRI based prostate cancer identification with random forests and auto-context model. Int Workshop Mach Learn Med Imaging 8679:314–322
180. Liu X, Langer DL, Haider MA, Yang Y, Wernick MN, Yetik IS (2009) Prostate cancer segmentation with simultaneous estimation of markov random field parameters and class. IEEE Trans Med Imaging 28(6):906–915
181. Sung YS, Kwon H-J, Park B-W, Cho G, Lee CK, Cho K-S, Kim JK (2011) Prostate cancer detection on dynamic contrast-enhanced mri: computer-aided diagnosis versus single perfusion parameter maps. Am J Roentgenol 197(5):1122–1129
182. Lopes R, Ayache A, Makni N, Puech P, Villers A, Mordon S, Betrouni N (2011) Prostate cancer characterization on MR images using fractal features. Med Phys 38(1):83–95
183. Mazzetti S, De Luca M, Bracco C, Vignati A, Giannini V, Stasi M, Russo F, Armando E, Agliozzo S, Regge D (2011) A CAD system based on multi-parametric analysis for cancer prostate detection on DCE-MRI. Proc SPIE 7963:79633Q
184. Parfait S, Walker PM, Créhange G, Tizon X, Mitéran J (2012) Classification of prostate magnetic resonance spectra using support vector machine. Biomed Signal Process Control 7(5):499–508
185. Kumar R, Indrayan A (2011) Receiver operating characteristic (ROC) curve for medical researchers. Indian Pediatr 48(4):277–287
186. Kelm BM, Menze BH, Zechmann CM, Baudendistel KT, Hamprecht FA (2007) Automated estimation of tumor probability in prostate magnetic resonance spectroscopic imaging: pattern recognition vs quantification. Magn Reson Med 57(1):150–159
187. Liu P, Wang S, Turkbey B, Grant K, Pinto P, Choyke P, Wood BJ, Summers RM (2013) A prostate cancer computer-aided diagnosis system using multimodal magnetic resonance imaging and targeted biopsy labels. Proc SPIE Int Soc Opt Eng 8670:86701G
188. Lv D, Guo X, Wang X, Zhang J, Fang J (2009) Computerized characterization of prostate cancer by fractal analysis in MR images. J Magn Reson Imaging 30(1):161–168
189. Tiwari P, Viswanath S, Kurhanewicz J, Sridhar A, Madabhushi A (2012) Multimodal wavelet embedding representation for data combination (MaWERiC): integrating magnetic resonance imaging and spectroscopy for prostate cancer detection. NMR Biomed 25(4):607–619
190. Khalvati F, Wong A, Haider MA (2015) Automated prostate cancer detection via comprehensive multi-parametric magnetic resonance imaging texture feature models. BMC Med Imaging 15(1):27
191. Sobecki P, Życka-Malesa D, Mykhalevych I, Sklinda K, Przelaskowski A (2017) MRI imaging texture features in prostate lesions classification. In: EMBEC and NBC 2017. Springer. pp. 827–830
192. Fehr D, Veeraraghavan H, Wibmer A, Gondo T, Matsumoto K, Vargas HA, Sala E, Hricak H, Deasy JO (2015) Automatic classification of prostate cancer Gleason scores from multiparametric magnetic resonance images. Proc Natl Acad Sci 112(46):E6265–E6273
193. Wibmer A, Hricak H, Gondo T, Matsumoto K, Moskowitz C, Fine SW, Reuter VE, Eastham J, Sala E, Vargas HA, "Haralick texture analysis of prostate MRI: utility for differentiating non-cancerous prostate from prostate cancer and differentiating prostate cancers with different Gleason scores. Eur Radiol 25:2840–2850
194. Vignati A, Mazzetti S, Giannini V, Russo F, Bollito E, Porpiglia F, Stasi M, Regge D (2015) Texture features on T2-weighted magnetic resonance imaging: new potential biomarkers for prostate cancer aggressiveness. Phys Med Biol 60(7):2685
195. Thibault G, Angulo J, Meyer F (2014) Advanced statistical matrices for texture characterization: application to cell classification. IEEE Trans Biomed Eng 61(3):630–637
196. Sun C, Wee WG (1983) Neighboring gray level dependence matrix for texture classification. Comput Vision Graph Image Process 23(3):341–352
197. Amadasun M, King R (1989)Textural features corresponding to textural properties. IEEE Trans Syst Man Cybern 19(5):1264–1274

198. García Molina JF, Zheng L, Sertdemir M, Dinter DJ, Schönberg S, Rädle M (2014) Incremental Learning with SVM for Multimodal Classification of Prostatic Adenocarcinoma. PLoS One 9(4):1–14
199. Duda D, Kretowski M, Mathieu R, de Crevoisier R, Bezy-Wendling J (2016) Multi-sequence texture analysis in classification of in vivo MR images of the prostate. Biocybern Biomed Eng 36(4):537–552
200. Yamin G, Schenker-Ahmed NM, Shabaik A, Adams D, Bartsch H, Kuperman J, White NS, Rakow-Penner RA, McCammack K, Parsons JK et al (2016) Voxel level radiologic–pathologic validation of restriction spectrum imaging cellularity index with Gleason grade in prostate cancer. Clin Cancer Res 22(11):2668–2674
201. Li X, Singanamalli A, Shanbhag D, Hötker AM, Aras O, Akin O, Bhagalia R (2016) Improved noninvasive prostate cancer assessment using multiparametric magnetic resonance imaging. In: biomedical imaging (ISBI), IEEE 13th international symposium on, 2016, pp. 1199–1203
202. Borren A, Groenendaal G, Moman MR, Boeken Kruger AE, Van Diest PJ, Van Vulpen M, Philippens MEP, Van Der Heide UA (2014) Accurate prostate tumour detection with multiparametric magnetic resonance imaging: dependence on histological properties. Acta Oncol (Madr) 53(1):88–95
203. Metzger GJ, Kalavagunta C, Spilseth B, Bolan PJ, Li X, Hutter D, Nam JW, Johnson AD, Henriksen JC, Moench L et al (2016) Detection of prostate cancer: quantitative multiparametric MR imaging models developed using registered correlative histopathology. Radiology 279(3):805–816
204. Riaz N, Afaq A, Akin O, Pei X, Kollmeier MA, Cox B, Hricak H, Zelefsky MJ (2012) Pretreatment endorectal coil magnetic resonance imaging findings predict biochemical tumor control in prostate cancer patients treated with combination brachytherapy and external-beam radiotherapy. Int J Radiat Oncol Biol Phys 84(3):707–711
205. Gnep K, Fargeas A, Gutiérrez-Carvajal RE, Commandeur F, Mathieu R, Ospina JD, Rolland Y, Rohou T, Vincendeau S, Hatt M et al (2017) Haralick textural features on T2-weighted MRI are associated with biochemical recurrence following radiotherapy for peripheral zone prostate cancer. J Magn Reson Imaging 45(1):103–117
206. Ginsburg SB, Rusu M, Kurhanewicz J, Madabhushi A (2014) Computer extracted texture features on T2w MRI to predict biochemical recurrence following radiation therapy for prostate cancer. Comput Aided Diagn 9035:903509
207. Park SY, Kim CK, Park BK, Lee HM, Lee KS (2011) Prediction of biochemical recurrence following radical prostatectomy in men with prostate cancer by diffusion-weighted magnetic resonance imaging: initial results. Eur Radiol 21(5):1111–1118
208. Woo S, Kim SY, Cho JY, Kim SH (Apr. 2016) Preoperative evaluation of prostate cancer aggressiveness: using ADC and ADC ratio in determining Gleason score. Am J Roentgenol 207(1):114–120
209. Donati OF, Mazaheri Y, Afaq A, Vargas HA, Zheng J, Moskowitz CS, Hricak H, Akin O (2014) Prostate cancer aggressiveness: assessment with whole-lesion histogram analysis of the apparent diffusion coefficient. Radiology 271(1):143–152
210. Fehr D, Veeraraghavan H, Wibmer A, Gondo T, Matsumoto K, Vargas HA, Sala E, Hricak H, Deasy JO (2015) Automatic classification of prostate cancer Gleason scores from multiparametric magnetic resonance images. Proc Natl Acad Sci 112:E6265–E6273
211. Rozenberg R, Thornhill RE, Flood TA, Hakim SW, Lim C, Schieda N (Feb. 2016) Whole-tumor quantitative apparent diffusion coefficient histogram and texture analysis to predict gleason score upgrading in intermediate-risk $3 + 4 = 7$ prostate cancer. Am J Roentgenol 206(4):775–782
212. Nketiah G, Elschot M, Kim E, Teruel JR, Scheenen TW, Bathen TF, Selnæs KM (2016) T2-weighted MRI-derived textural features reflect prostate cancer aggressiveness: preliminary results. Eur Radiol 27:1–10,
213. Wang XZ, Wang B, Gao ZQ, Liu JG, Liu ZQ, Niu QL, Sun ZK, Yuan YX (2009) Diffusion-weighted imaging of prostate cancer: correlation between apparent diffusion coefficient values and tumor proliferation. J Magn Reson Imaging 1366:1360–1366
214. Langer DL, Evans AJ, Plotkin A, Trachtenberg J, Wilson BC, Haider MA (2010) Prostate tissue composition and mr measurements: investigating the relationships between ADC, T2, Ktrans, Ve and corresponding histologic features. Radiology 255(2):485–494
215. Kuo MD, Jamshidi N (2014) Behind the numbers: decoding molecular phenotypes with radiogenomics—guiding principles and technical considerations. Radiology 270(2):320–325
216. Incoronato M, Aiello M, Infante T, Cavaliere C, Grimaldi AM, Mirabelli P, Monti S, Salvatore M (2017) Radiogenomic analysis of oncological data: a technical survey. Int J Mol Sci 18(4):805–832
217. Jamshidi N, Margolis DJ, Raman S, Huang J, Reiter RE, Kuo MD (2017) Multiregional radiogenomic assessment of prostate microenvironments with multiparametric MR imaging and DNA whole-exome sequencing of prostate glands with adenocarcinoma. Radiology 284:162827
218. Stoyanova R, Pollack A, Takhar M, Lynne C, Parra N, Lam LLC, Alshalalfa M, Buerki C, Castillo R, Jorda M et al (2016) Association of multiparametric MRI quantitative imaging features with prostate cancer gene expression in MRI-targeted prostate biopsies. Oncotarget 7(33):53362
219. Stoyanova R, Takhar M, Tschudi Y, Ford JC, Solórzano G, Balagurunathan Y, Punnen S, Davicioni E, Gillies RJ, Pollack A (2016) Prostate cancer radiomics and the promise of radiogenomics. Trans Cancer Res 5(4):432–447
220. Ragnum HB, Vlatkovic L, Lie AK, Axcrona K, Julin CH, Frikstad KM, Hole KH, Seierstad T, Lyng H (2015) The tumour hypoxia marker pimonidazole reflects a transcriptional programme associated with aggressive prostate cancer. Br J Cancer 112(2):382–390
221. McCann SM, Jiang Y, Fan X, Wang J, Antic T, Prior F, VanderWeele D, Oto A (2016) Quantitative multiparametric MRI features and PTEN expression of peripheral zone prostate cancer: a pilot study. Am J Roentgenol 206(3):559–565
222. Kuhn M (2008) Building Predictive Models in R Using the caret Package. J Stat Softw 28(5):1–26
223. Dormann CF, Elith J, Bacher S, Buchmann C, Carl G, Carr G, Garc JR, Gruber B, Lafourcade B, Leit PJ, Tamara M, Mcclean C, Osborne PE, Der BS, Skidmore AK, Zurell D, Lautenbach S (2012) Collinearity: a review of methods to deal with it and a simulation study evaluating their performance. Ecography 36:27–46
224. Crone SF, Finlay S (2012) Instance sampling in credit scoring: an empirical study of sample size and balancing. Int J Forecast 28(1):224–238
225. Chawla NV, Bowyer KW, Hall LO, Kegelmeyer WP (2002) SMOTE: synthetic minority over-sampling technique. J Artif Intell Res 16:321–357
226. Chandana S, Leung H, Trpkov K (2009) Staging of prostate cancer using automatic feature selection, sampling and dempster–shafer fusion. Cancer Informatics 7:57–73